Mechanics of Materials 40 (2008) 885–906

Contents lists available at ScienceDirect

Mechanics of Materials

journal homepage: www.elsevier.com/locate/mechmat

A micro-macromechanical approach for composite laminates

Mario W.E. Toledo [a,*], Liz G. Nallim [a,b], Bibiana M. Luccioni [b,c]

[a] ICMASa, Facultad de Ingeniería, Universidad Nacional de Salta, Avenida Bolivia 5150, 4400 Salta, Argentina
[b] CONICET, Avenida Rivadavia 1917, CP C1033AAJ, Ciudad de Buenos Aires, Argentina
[c] Instituto de Estructuras, Universidad Nacional de Tucumán, Avenida Roca 1800, S.M. de Tucumán, Argentina

ARTICLE INFO

Article history:
Received 22 August 2006
Received in revised form 7 May 2008

Keywords:
Composites
Laminates
Fibers
Plasticity
Anisotropy
Finite elements

ABSTRACT

The calibration of a general model for composite materials and its application to the case of fiber reinforced composite laminates are presented in this paper. The constitutive equation for the composite results from the combination of the constitutive equations of the laminae that, in turn, are obtained from the combination of fibers and matrix. The behavior of each component is simulated by a general elastoplastic anisotropic model. The combination rules obey to the microstructure of the composite. In order to calibrate the general model, the behavior of composites formed by laminae reinforced with unidirectional fibers is studied. Three-dimensional finite element models are used to study the distribution of stresses and strains inside the composite. These finite element models are useful to verify the hypotheses of the proposed composites theory, in a relatively simple way. Comparisons between elastic properties of laminae obtained with the finite elements model, with Mori–Tanaka method, with the model for composite studied and experimental results are included in the paper. Elastic properties of laminates with different stacking sequences and fibers orientations are also obtained. Additionally, application examples showing the non-linear response of laminae and laminates obtained with the calibrated model and comparisons with experimental results are presented. The results show that the calibrated model describes the behavior up to failure of composite laminates. The failure mode of the composite produced by the failure of one or more of its components can be identified. The calibrated model is also able to reproduce complex failure modes that change from the matrix to the fibers depending on the type of stress state.

1. Introduction

In recent years, conventional materials are continuously being replaced by a variety of composite materials. This fact has caused an increasing interest on the modeling of composites. Several approaches have been developed but there is still a strong need of predicting models that can be used for stiffness and strength assessment of this type of materials in practical situations (Wang and Yan, 2005).

Constitutive models for fiber reinforced composite laminates can be classified according to the scale in which they are defined (Chaboche et al., 1998). In macro-models the composite material is represented as a unique material with average properties. This type of approach is generally not able to describe the overall inelastic behavior and failure behavior of laminates.

In meso-models the composite is assumed to be formed by unidirectional laminae for which macroscopic equations are derived. The constitutive properties of individual laminae are obtained from experimental tests (Huang, 2001). Many meso-models including several non-linear phenomena like fiber microbuckling (Basu et al., 2007), plasticity with different non-linear response in tension and compression (Yokozeki et al., 2007), damage due to matrix dominated failure modes (Schuecker and

* Corresponding author. Tel./fax: +54 0387 4255351.
E-mail address: mwtoledo@unsa.edu.ar (M.W.E. Toledo).

0167-6636/$ - see front matter © 2008 Elsevier Ltd. All rights reserved.
doi:10.1016/j.mechmat.2008.05.004

Pettermann, 2006) damage due to intralaminar failure mechanisms (Maimí et al., 2007a,b), fiber failure and inter fibre failure (Knops and Bögle, 2006) have been recently proposed.

In contrast to meso-models, micro-models use the constitutive equations of the elemental constituents: matrix, fibers, interfaces, etc. This approach has the advantage of allowing the identification of the failure mode but requires accurate experimental data for the individual components, which are not generally available.

Many micro-models have been proposed recently to model different phenomena taking place at the micro-level. Narayana Naik et al. (2005) presented a new failure theory for laminated based on micro-mechanical analysis of composites, wherein a representative volume consists of a fiber surrounded by matrix in appropriate volume fraction. Bonora and Ruggiero (2006a,b) modeled the matrix-reinforcement assembly process including mechanical interfaces in addition to fiber failure, ductile damage for the matrix progressive failure and fiber–matrix debonding. Lee and Kim (2007) implemented a micro-mechanical constitutive model developed by Liang et al. (2006), based on the concept of the ensemble-volume average for laminated composites, to numerically characterize the compressive response and damage evolution in laminated composites.

Most of the theories developed at the micro-level are generally too complicated or, when they are simple, they are only able to reproduce a few aspects of the behavior in fiber directions or they are only valid for composites in which stiffness and strength of the fibers are significantly greater than those of the matrix (Huang, 2001).

An alternative approach is the use of multi-scale models (Oller et al., 2005; Zhu et al., 2006). Tay-Earn et al. (2006) presented a new micro–macro approach to model damage and fracture of composites.

Recently Hinton and Soden, organized a 'failure exercise' to compare the predictive capabilities of a number of the most important strength theories for laminated composites in current usage (Hinton and Soden, 1998; Soden et al., 1998a, 2002; Hinton et al., 2002, 2004a). The results of that exercise (Soden et al., 1998b, 2004; Kaddour et al., 2004; Hinton et al., 2004b) were used for the assessment of the accuracy of current theoretical methods of failure prediction in composite laminates.

A numerical model for general composite materials (Luccioni, 2006), appropriate for the mechanical analysis of fiber reinforced composite laminates, is calibrated in this paper. The model is developed under the assumption of small strains and is based on an analysis at component materials level. At a first stage, the behavior of an individual lamina is obtained from the mechanical properties of matrix and fibers, their volume ratio and their orientation. Then, the behavior of the laminate can be reproduced composing laminae with different fiber orientations. The final equations of the model are similar to those of 'bridging models' (Huang, 2007). The model is completely general and can be used for other types of composite materials.

2. Constitutive model

2.1. Introduction

The model used in this paper is based on very simple kinematical and equilibrium assumptions that, properly handled, lead to the composite constitutive equation and to the strain and stress tensors in all the components. These assumptions result from the microstructure of the composite. In this way, departing from the behavior of fibers and matrix, the elastic properties of the laminate can be obtained and the non-linear behavior and the progressive failure can be analyzed.

2.2. Constitutive model for the components

It is well known that fibers present a strong anisotropic behavior generally assumed as transversely isotropic, characterized not only by the elastic orthotropy like in the case of carbon fibers, but also by the marked difference of strength in the principal directions. Another important property of fibers is their slightly lower strength in compression than in tension.

In general, epoxy resins have lower tension than compression strength like brittle materials. In the case of polymeric matrix the material itself can be considered as an isotropic material. Nevertheless, as the fiber/matrix interface is not explicitly modeled, the constitutive model of the matrix is modified including the interface constitutive model (Luccioni and López, 2002, 2005). Orthotropic elastoplastic or damage interface models can be used to simulate fiber debonding or delamination. As a result, the constitutive model of the matrix including the interface exhibits tension strength much lower in perpendicular direction to fiber than in longitudinal direction.

Taking into account the above considerations, each one of the basic components is supposed to have a general orthotropic elastoplastic behavior covering the case of fibers, matrix and interface included in matrix (Luccioni, 2006).

The orthotropic model used is based on the assumption that two spaces can be defined (Betten (1988); Luccioni et al., 1995): (a) A real anisotropic space and (b) a fictitious isotropic space. The problem is solved in the fictitious isotropic space allowing the use of elastoplastic models originally developed for isotropic materials. The isotropic elastoplastic model used in this paper includes energy-based criteria to make it suitable for brittle materials (Oller et al., 1995; Luccioni et al., 1995).

Stress tensors in both spaces are related by a tensor transformation that can be written as,

$$\boldsymbol{\tau} = \boldsymbol{A}(\boldsymbol{\sigma}, \kappa^{p}) : \boldsymbol{\sigma} \tag{1}$$

where $\boldsymbol{\tau}$ and $\boldsymbol{\sigma}$ are the stress tensors in spaces (a) and (b) respectively, and $\boldsymbol{A}$ is a fourth order transformation tensor that contains the information about strength anisotropy depending on material symmetry. In the most general case, this tensor varies with the stress state and the evolution of the inelastic process represented by the isotropic plastic hardening variable κ^{p} (Luccioni et al., 1996). In this paper,

all the components materials are assumed initially orthotropic with three axes of material symmetry. There are different alternatives to define tensor $\boldsymbol{A}$ for this case (Oller et al., 1995; Luccioni et al., 1996; Luccioni and Martín, 1997; Car et al., 1999; Oller et al., 2003). The simplest way is a diagonal fourth order tensor (Luccioni et al., 1995),

$$A_{ijkl} = \sum_{m=1}^{3}\sum_{n=1}^{3} \delta_{im}\delta_{jn}\delta_{km}\delta_{\ln}\bar{\tau}/\bar{\sigma}_{mn} \tag{2}$$

where $\bar{\tau}$ is the strength in the fictitious isotropic space and $\bar{\sigma}_{mn}$ is the actual strength in the direction m in the plane with normal n. A better approach has been proposed by Oller et al. (2003).

The plastic threshold is defined through a yielding function,

$$F(\boldsymbol{\sigma};\boldsymbol{\alpha}) = \overline{F}(\boldsymbol{\tau};\bar{\boldsymbol{\alpha}}) = 0 \tag{3}$$

where F and $\overline{F}$ represent the yielding function in the real anisotropic space and the fictitious isotropic space respectively; $\boldsymbol{\alpha}$ and $\bar{\boldsymbol{\alpha}}$ are plastic internal variables in correspondence with both spaces.

The transformation defined by Eq. (1) allows the use of yielding functions $\overline{F}$ defined for isotropic materials in the fictitious isotropic space. It should be noted that this space is isotropic with respect to yielding thresholds and strength but not necessarily with respect to other properties like elastic stiffness.

Evolution of plastic strain in real space is defined with the well-known flow rule,

$$\dot{\boldsymbol{\varepsilon}}^{\mathrm{p}} = \dot{\lambda}(\partial G/\partial\boldsymbol{\sigma}) \tag{4}$$

where G is the plastic potential function defined in the real stress space. Instead of working with this function that should be anisotropic, function $\overline{G}$ defined in the fictitious isotropic space could be used.

$$G(\boldsymbol{\sigma},\boldsymbol{\alpha}) = \overline{G}(\boldsymbol{\tau},\bar{\boldsymbol{\alpha}}) \tag{5}$$

Eq. (4) can be then rewritten as,

$$\dot{\boldsymbol{\varepsilon}}^{\mathrm{p}} = \dot{\lambda}(\partial\overline{G}/\partial\boldsymbol{\sigma}) = \dot{\lambda}(\partial\overline{G}/\partial\boldsymbol{\tau}) : (\partial\boldsymbol{\tau}/\partial\boldsymbol{\sigma}) = \dot{\lambda}(\partial\overline{G}/\partial\boldsymbol{\tau}) : \boldsymbol{H} = \dot{\lambda}\bar{\boldsymbol{h}}$$
$$\text{with } \boldsymbol{H} = \partial\boldsymbol{\tau}/\partial\boldsymbol{\sigma} \text{ and } \bar{\boldsymbol{h}} = (\partial\overline{G}/\partial\boldsymbol{\tau}) : \boldsymbol{H} \tag{6}$$

where $\boldsymbol{H}$ is a fourth-rank tensor and $\bar{\boldsymbol{h}}$ is a second-rank tensor and represents the plastic flow in the real orthotropic space.

The constitutive equations for the components can be written as follows:

$$\boldsymbol{\sigma} = \mathbf{C} : \boldsymbol{\varepsilon}^{\mathrm{e}} = \mathbf{C} : (\boldsymbol{\varepsilon} - \boldsymbol{\varepsilon}^{\mathrm{p}}), \tag{7}$$

where $\boldsymbol{\sigma}$ is the stress tensor, $\mathbf{C}$ is the elastic stiffness tensor, $\boldsymbol{\varepsilon}^{\mathrm{e}}$ is the elastic strain tensor, $\boldsymbol{\varepsilon}$ is the strain tensor and $\boldsymbol{\varepsilon}^{\mathrm{p}}$ is the plastic or inelastic strain tensor.

If a 'simple composite' is analyzed with respect to its principal directions, some directions in which all the components have the same strain (parallel behavior) and other directions in which all the components have the same stress (series behavior) can be identified. In correspondence to each stress or strain tensor component a parallel or series behavior can be assumed. A parallel behavior in correspondence with one component means that all the composite constituents have the same value for this strain component. A series behavior in correspondence with one component means that all the composite constituents have the same value for this stress component.

Based on this analysis, stress and strain components could be rearranged. Tensor $\boldsymbol{\varepsilon}^{*}$ contains strain components in correspondence with directions of parallel behavior and stress components in correspondence with directions of series behavior, and $\boldsymbol{\sigma}^{*}$ contains stress components in correspondence with directions of parallel behavior and strain components in correspondence with directions of series behavior.

In order to express this rearrangement the following fourth order tensors are defined,

$$\alpha^{\sigma}_{ijkl} = \sum_{r=1}^{3}\sum_{s=1}^{3} \delta_{ir}\delta_{js}\delta_{kr}\delta_{ls}H(p_{rs}) \quad \text{with} \quad \alpha^{\varepsilon}_{ijkl} = \delta_{ik}\delta_{jl} - \alpha^{\sigma}_{ijkl} \tag{8}$$

$$p_{rs} = \begin{cases} 1 \text{ if the } rs \text{ component works in parallel} \\ 0 \text{ if the } rs \text{ component works in series} \end{cases}$$

H: Threshold function

Stress and strain components are rearranged as follows,

$$\boldsymbol{\sigma}^{*} = \boldsymbol{\alpha}^{\sigma} : \boldsymbol{\sigma} + \boldsymbol{\alpha}^{\varepsilon} : \boldsymbol{\varepsilon} \quad \boldsymbol{\varepsilon}^{*} = \boldsymbol{\alpha}^{\varepsilon} : \boldsymbol{\sigma} + \boldsymbol{\alpha}^{\sigma} : \boldsymbol{\varepsilon} \quad \text{and} \quad \boldsymbol{\sigma} = \boldsymbol{\alpha}^{\sigma} : \boldsymbol{\sigma}^{*} + \boldsymbol{\alpha}^{\varepsilon} : \boldsymbol{\varepsilon}^{*} \quad \boldsymbol{\varepsilon} = \boldsymbol{\alpha}^{\varepsilon} : \boldsymbol{\sigma}^{*} + \boldsymbol{\alpha}^{\sigma} : \boldsymbol{\varepsilon}^{*} \tag{9}$$

Combining Eqs. (7) and (9), the secant constitutive relation for the components can be alternatively written as,

$$\boldsymbol{\sigma}^{*} = \mathbf{C}^{*} : \boldsymbol{\varepsilon}^{*} - \boldsymbol{\sigma}^{\mathrm{p}^{*}} \tag{10}$$

where

$$\mathbf{C}^{*} = (\boldsymbol{\alpha}^{\sigma} : \mathbf{C} + \boldsymbol{\alpha}^{\varepsilon}) : (\boldsymbol{\alpha}^{\varepsilon} : \mathbf{C} + \boldsymbol{\alpha}^{\sigma})^{-1} \tag{11}$$

$$\boldsymbol{\sigma}^{\mathrm{p}^{*}} = (\mathbf{C}^{*} : \boldsymbol{\alpha}^{\sigma} - \boldsymbol{\alpha}^{\varepsilon}) : \boldsymbol{\varepsilon}^{\mathrm{p}} \tag{12}$$

Actually $\boldsymbol{\sigma}^{\mathrm{p}^{*}}$ is a plastic corrector for the modified stress tensor. It is a tensor that contains plastic corrector stress components in correspondence with components working in series and plastic strain components affected with minus sign in correspondence with components working in series.

2.3. Composite constitutive equation

The case of a composite with simple structure, where principal directions and tensors $\boldsymbol{\alpha}^{\boldsymbol{\sigma}}$ and $\boldsymbol{\alpha}^{\boldsymbol{\varepsilon}}$ are coincident for all the constituents, is first analyzed. In such a composite the following condition is verified,

$$\boldsymbol{\varepsilon}^{*}_{c} = \boldsymbol{\varepsilon}^{*} \tag{13}$$

where c indicates an arbitrary material component.

Assuming that the plastic strain of the composite in the directions in which the material works in series can be obtained as the sum of the plastics strains of the components multiplied by their respective volume fractions, the following secant equation is obtained,

$$\boldsymbol{\sigma}^{*} = \mathbf{C}^{*} : \boldsymbol{\varepsilon}^{*} - \boldsymbol{\sigma}^{\mathrm{p}^{*}} \tag{14}$$

where

$$\mathbf{C}^{*} = \sum k_c \mathbf{C}_c^{*}, \quad \boldsymbol{\sigma}^{\mathrm{p}^{*}} = \sum k_c \boldsymbol{\sigma}_c^{\mathrm{p}^{*}} = \sum k_c (\mathbf{C}_c^{*} : \boldsymbol{\alpha}^{\sigma} - \boldsymbol{\alpha}^{\varepsilon}) : \boldsymbol{\varepsilon}_c^{\mathrm{p}} \tag{15}$$

and k_c represents the volume fraction of a generic constituent material.

Eq. (14) can be rearranged with the aid of Eq. (9) to give,

$$\boldsymbol{\sigma} = \mathbf{C} : \boldsymbol{\varepsilon} - \boldsymbol{\sigma}^{\mathrm{p}} \tag{16}$$

where

$$\mathbf{C} = (\boldsymbol{\alpha}^{\sigma} : \mathbf{C}^{*} + \boldsymbol{\alpha}^{\varepsilon}) : (\boldsymbol{\alpha}^{\varepsilon} : \mathbf{C}^{*} + \boldsymbol{\alpha}^{\sigma})^{-1}$$
$$\boldsymbol{\sigma}^{\mathrm{p}} = -\mathbf{C} : \boldsymbol{\alpha}^{\varepsilon} : \boldsymbol{\sigma}^{\mathrm{p}^{*}} + \boldsymbol{\alpha}^{\sigma} : \boldsymbol{\sigma}^{\mathrm{p}^{*}} = (\boldsymbol{\alpha}^{\sigma} - \mathbf{C} : \boldsymbol{\alpha}^{\varepsilon}) : \boldsymbol{\sigma}^{\mathrm{p}^{*}} \tag{17}$$

Numerical implementation in a finite element program requires the evaluation of the strain tensor for each one of the components from the composite strains. In this way, once the strains are known, constitutive equations can be independently integrated for each constituent and information at the constituents material level (fiber and matrix) can be recorded through the corresponding internal variables.

Starting from condition (13) and Eqs. (9) and (16), the following relation can be written,

$$\boldsymbol{\varepsilon}_c = \boldsymbol{\phi}_c : \boldsymbol{\varepsilon} + \tilde{\boldsymbol{\varepsilon}}_c^{\mathrm{p}} \tag{18}$$

where

$$\boldsymbol{\phi}_c = (\boldsymbol{\alpha}^{\varepsilon} : \mathbf{C}_c^{*} + \boldsymbol{\alpha}^{\sigma}) : (\boldsymbol{\alpha}^{\varepsilon} : \mathbf{C}^{*} + \boldsymbol{\alpha}^{\sigma})^{-1}; \ \tilde{\boldsymbol{\varepsilon}}_c^{\mathrm{p}} = \boldsymbol{\phi}_c : \boldsymbol{\alpha}^{\varepsilon} : \boldsymbol{\sigma}^{*\mathrm{p}} - \boldsymbol{\alpha}^{\varepsilon} : \boldsymbol{\sigma}_c^{*\mathrm{p}} \tag{19}$$

It is important to point out that all preceding equations are only valid in the composite local system of reference, which is coincident with its principal elasticity symmetry directions. For an arbitrary reference system, all tensors must be rotated.

The constitutive equations for a laminated composite or for a composite material with a more complex structure, where tensors $\boldsymbol{\alpha}^{\boldsymbol{\sigma}}$ and $\boldsymbol{\alpha}^{\boldsymbol{\varepsilon}}$ are not the same for all components, can be obtained in different steps. The composite must be decomposed in more simple sub-composites for which the corresponding constitutive equations can be obtained as described above. Then, the constitutive equation of the composite can be written with a similar approach

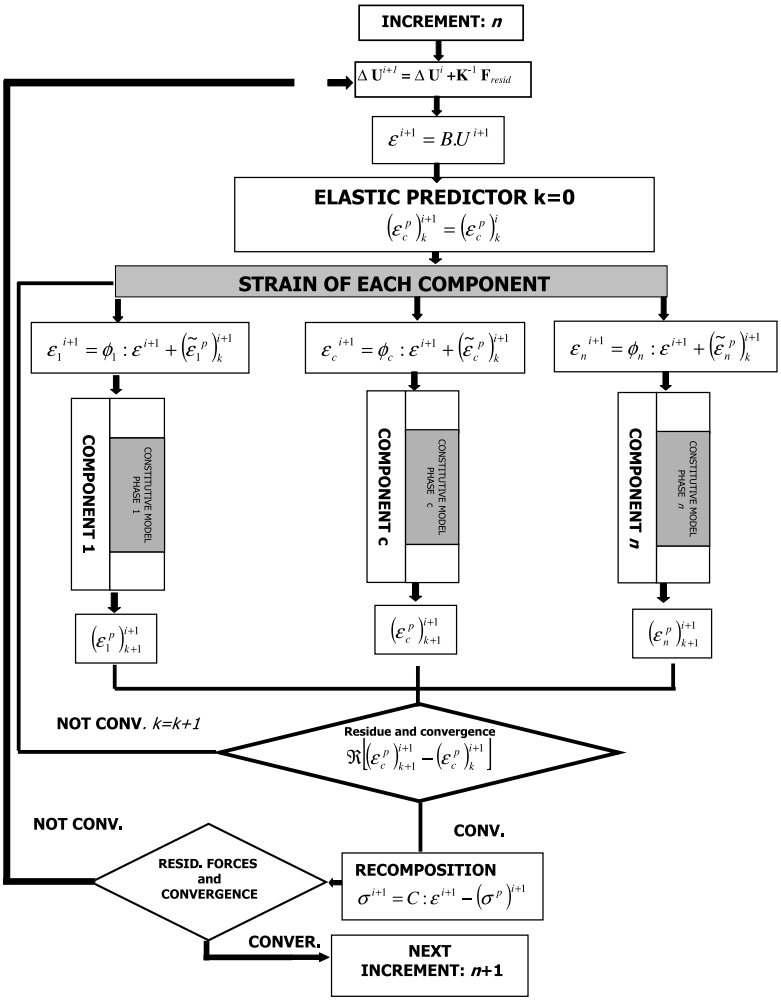

Fig. 1. Numerical algorithm.

composing the constitutive equations already found for the sub-components.

2.4. Numerical implementation

The model presented can be implemented in a non-linear finite element program using the iterative scheme presented in Fig. 1. Strains in each component can be evaluated with Eq. (18) if plastic strains are known. In case of a more complex composite, this scheme must be used to decompose the composite in sub-composites and again inside each sub-composite to arrive to each one of the constituents.

In any case, plastic strains of all components are required for the evaluation of the strains in each component. As a result, the problem cannot be explicitly solved and, for example, an iterative scheme must be used. The algorithm schematized in Fig. 1 is based on a predictor-corrector iterative procedure using the norm of plastic strains as convergence measure. The algorithm is very stable. No more than two iterations were required to correct the strain distribution in plastic regime for all application examples presented in this paper.

Once the strains of each one of the constituents have been obtained, the correspondent constitutive equations can be integrated using well-known procedures like Euler Backward or return mapping algorithms.

3. Model calibration

3.1. Introduction

The constitutive model presented in the previous section assumes that each component can be successively subdivided into sub-components, until arriving to simple composites in which kinematical and equilibrium assumptions among simple components can be established. It is assumed that, in simple composites the components can work in series or in parallel in correspondence with each one of the stress or strain components. The elements of tensors $\boldsymbol{\alpha}^{\boldsymbol{\sigma}}$ and $\boldsymbol{\alpha}^{\boldsymbol{\varepsilon}}$ must be prescribed according to the components behavior.

The main purpose of this study is to calibrate the proposed theoretical model for fiber composite laminates. In order to determine the elements of tensors $\boldsymbol{\alpha}^{\boldsymbol{\sigma}}$ and $\boldsymbol{\alpha}^{\boldsymbol{\varepsilon}}$, the distribution of stresses and strains inside a simple composite by means of a linear elastic analysis is performed in this section. According to the model described in the previous section, tensors $\boldsymbol{\alpha}^{\boldsymbol{\sigma}}$ and $\boldsymbol{\alpha}^{\boldsymbol{\varepsilon}}$ are constant and, therefore, they can be determined in elastic regimen. Taken into account that the elastic deformations in fiber–matrix or lamina–lamina interfaces are worthless, they were not considered in the present analysis.

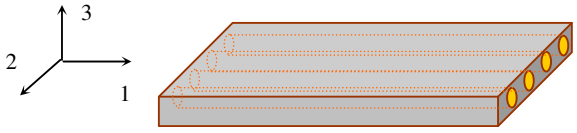

Fig. 2. Unidirectional fiber reinforced composite.

3.2. Unidirectional lamina

A micro-mechanical study of the elastic properties of laminae reinforced with unidirectional long fibers is presented in this section. The analysis is carried out by means of finite element models and applying the theory developed by Eshelby (1957) together with the interaction effects of Mori and Tanaka (1973).

Fibers of circular section, regularly spaced, aligned and perfectly bonded to matrix are considered. The matrix is supposed to be isotropic itself and free of holes and imperfections.

The study is carried out for different types of laminae. All of them are laminae reinforced with unidirectional fibers as it is schematized in Fig. 2 where local axes are also indicated. Mechanical properties of fiber and matrix components for different laminae are presented in Table 1 (Soden et al., 1998a).

3.2.1. Micro-model of finite elements

For the micro-mechanical study of elastic properties of an unidirectional lamina, representative models of the

Table 1
Elastic properties of fibers and matrices (Soden et al., 1998a)

Lamina	Properties of fibers	Properties of matrices
1	Fiber type: E-glass $E_f = 73.1$ GPa $\nu_f = 0.22$	Matrix type: epoxi $E_m = 3.45$ GPa $\nu_m = 0.35$
2	Fiber type: carbon $E_{f1} = 232$ GPa $E_{f2} = 15$ GPa $G_{f12} = 24$ GPa $\nu_{f12} = 0.279$ $\nu_{f23} = 0.49$	Matrix type: epoxi $E_m = 5.35$ GPa $\nu_m = 0.35$
3	Fiber type: AS4 (carbon) $E_{f1} = 225$ GPa $E_{f2} = 15$ GPa $G_{f12} = 15$ GPa $\nu_{f12} = 0.2$ $\nu_{f23} = 0.25$	Matrix type: 3501-6 epoxi $E_m = 4.2$ GPa $\nu_m = 0.34$ $G_m = 1.567$ GPa
4	Fiber type: T300 (carbon): $E_{f1} = 230$ GPa $E_{f2} = 15$ GPa $G_{f12} = 15$ GPa $\nu_{f12} = 0.2$ $\nu_{f23} = 0.25$	Matrix type: BSL914C epoxi $E_m = 4.0$ GPa $\nu_m = 0.35$ $G_m = 1.481$ GPa
5	Fiber type: E-glass 21xK43 Gevetex $E_{f1} = 80$ GPa $E_{f2} = 80$ GPa $G_{f12} = 33.33$ GPa $\nu_{f12} = 0.2$ $\nu_{f23} = 0.2$	Matrix type: LY556/HT907/DY063 epoxi $E_m = 3.35$ GPa $\nu_m = 0.35$, $G_m = 1.24$ GPa
6	Fiber type: Silenka E-Glass 1200tex: $E_{f1} = 74$ GPa $E_{f2} = 74$ GPa. $G_{f12} = 30.8$ GPa $\nu_{f12} = 0.2$ $\nu_{f23} = 0.2$	Matrix type: MY750/HY917/DY063 epoxi $E_m = 3.35$ GPa. $\nu_m = 0.35$ $G_m = 1.24$ GPa
7	Fiber type: E-glass $E_{f1} = 72.4$ GPa $E_{f2} = 72.4$ GPa $G_{f12} = 30.2$ GPa $\nu_{f12} = 0.2$ $\nu_{f23} = 0.2$	Matrix type: epoxi $E_m = 2.76$ GPa. $\nu_m = 0.35$

lamina structure with different fiber proportions were built.

The finite element analysis was carried out with the program SAP 2000 Advanced 9.0.3 (CSI Analysis Reference Manual, 2004) and 3D solid elements were used to model the composite structure. The boundary conditions and the applied displacements considered for the determination of the longitudinal Young modulus E_1 (Fig. 3a) and the transverse elastic modulus G_{12} (Fig. 3b) are shown in the Fig. 3.

In order to identify and eliminate errors introduced by the mesh size, different mesh sizes were used and the results were compared. An unidirectional lamina with a fibers volume fraction $k_f = 0.6$, identified as Lamina 3 in Table 1 was taken as witness case.

The values of the scaled elastic constants obtained with different mesh sizes are presented in Fig. 4. All elastic constants are scaled with the values corresponding to the finest mesh (2576 elements). An appropriate convergence of the results is obtained for the elastic moduli E_1, E_2, G_{12} and the Poisson ratio v_{23} but not the Poisson ratio v_{12}. The differences can be attributed to the simplification of considering an homogeneous medium for the determination of v_{12} when it is highly heterogeneous in the plane 1–2. From Fig. 4, it could be concluded that meshes of 1020 elements or more are accurate enough to describe the elastic behavior of laminae. The typical mesh with 1680 elements used in a fiber–matrix unit cell is illustrated in Fig. 5.

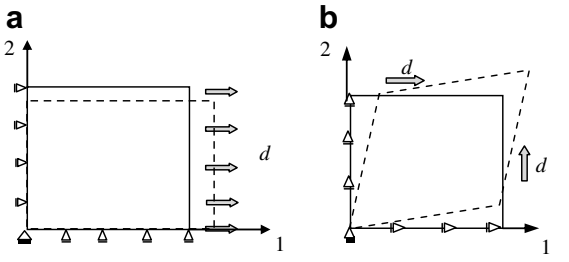

Fig. 3. Boundary conditions: (a) longitudinal Young modulus E_1; (b) shear Moduli G_{12}.

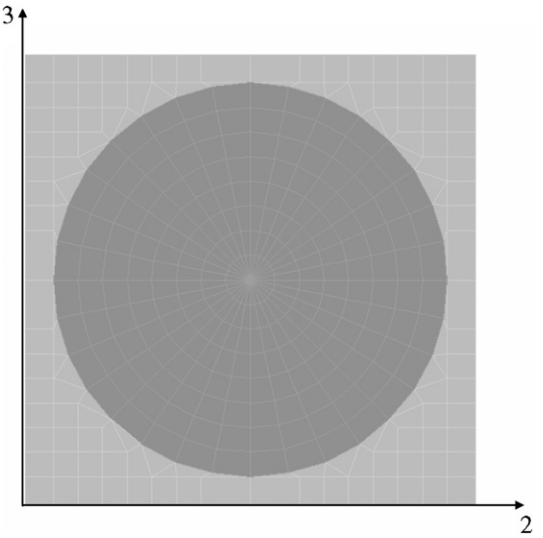

Fig. 5. Finite element mesh of a symmetric unit cell.

The distributions of stresses and strains obtained with the above described analysis, leads to the conclusion that fiber and matrix work in parallel in correspondence with the stress component $\boldsymbol{\sigma}_{11}$ and that for the component corresponding to the stress $\boldsymbol{\tau}_{23}$ fiber and matrix work in series. In correspondence with the components $\boldsymbol{\sigma}_{22}$ and $\boldsymbol{\tau}_{12}$, the behavior cannot be considered neither completely in series nor completely in parallel.

3.2.2. Application of Mori–Tanaka method

The micro-mechanics based Mori–Tanaka method (Mori and Tanaka, 1973; Benveniste, 1985) is used in this section to predict the elastic mechanical properties of the unidirectional laminae depicted in Table 1. This method may be viewed as the simplest mean field approach for inhomogeneous materials that encompass the full physical range of phase volume fraction.

Eshelby's results (Eshelby, 1957) show that if an elastic homogeneous ellipsoidal inclusion in an infinite linear

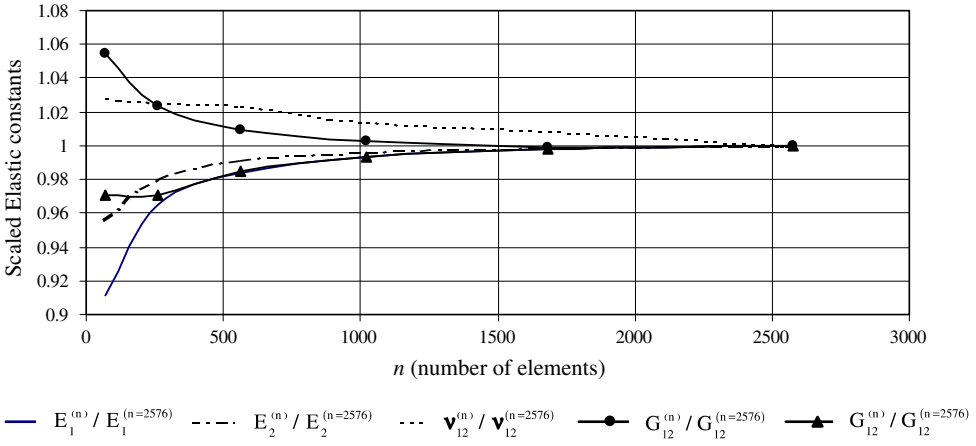

Fig. 4. Variation of scaled elastic properties with different mesh sizes.

elastic matrix is subjected to a eigenstrain $\boldsymbol{\varepsilon}^{\mathrm{T}}$, uniform strain states $\boldsymbol{\varepsilon}^{\mathrm{C}}$ is induced and it is related to the eigenstrain by the expression

$$\boldsymbol{\varepsilon}^{\mathrm{C}} = \mathbf{S}^{\mathrm{E}} : \boldsymbol{\varepsilon}^{\mathrm{T}} \tag{20}$$

where $\mathbf{S}^{\mathrm{E}}$ is the Eshelby tensor, which depends on the reinforcement dimensions and the Poisson ratio of the matrix v_{m}. The components of this tensor for a circular, cylindrical inclusion with an infinite length-to-diameter ratio parallel to the 1-axis, are obtained in this paper

$$\begin{aligned} &S_{1111} = S_{1133} = S_{1122} = 0, \quad S_{3333} = S_{2222} = \frac{5 - 4v_{\mathrm{m}}}{8(1 - v_{\mathrm{m}})}, \\ &S_{3322} = S_{2233} = \frac{4v_{\mathrm{m}} - 1}{8(1 - v_{\mathrm{m}})} \\ &S_{3311} = S_{2211} = \frac{v_{\mathrm{m}}}{2(1 - v_{\mathrm{m}})}, \quad S_{3232} = \frac{3 - 4v_{\mathrm{m}}}{8(1 - v_{\mathrm{m}})}, \\ &S_{1313} = S_{1212} = \frac{1}{4} \end{aligned} \tag{21}$$

Eshelby (1957) introduced the concept of the equivalent homogeneous inclusion for inhomogeneous inclusions. This concept as well as the effects of the interaction among the inclusions defined by Mori and Tanaka (1973), allow to obtain the transformation strains in order to equal the total stresses in the inhomogeneities and their equivalent inclusions, as described in the following equation

$$\mathbf{C}_{\mathrm{f}} : (\boldsymbol{\varepsilon}^{a} + \boldsymbol{\varepsilon}^{\mathrm{int}} + \boldsymbol{\varepsilon}^{\mathbf{C}}) = \mathbf{C}_{\mathrm{m}} : (\boldsymbol{\varepsilon}^{a} + \boldsymbol{\varepsilon}^{\mathrm{int}} + \boldsymbol{\varepsilon}^{\mathbf{C}} - \boldsymbol{\varepsilon}^{\mathbf{T}}) \tag{22}$$

where $\mathbf{C}_{\mathrm{f}}$ and $\mathbf{C}_{\mathrm{m}}$ are the stiffness tensors of fiber and matrix, respectively; $\boldsymbol{\varepsilon}^{a}$ is the uniform far field strain applied to the domain at infinity, $\boldsymbol{\varepsilon}^{\mathrm{int}}$ is the average elastic strain defined by Mori and Tanaka (1973) which is given by

$$\boldsymbol{\varepsilon}^{\mathrm{int}} = -k_{\mathrm{f}}(\boldsymbol{\varepsilon}^{\mathrm{C}} - \boldsymbol{\varepsilon}^{\mathrm{T}}) \tag{23}$$

Finally, the stiffness tensor $\mathbf{C}$ for different unidirectional laminae can be obtained from energy considerations. Many authors gave different but essentially equivalent Mori–Tanaka expressions for the effective elastic tensor of inhomogeneous materials. Alternatively, the method above described can be used (Tandon and Weng, 1984) to directly evaluate the overall elasticity tensor as

$$\mathbf{C} = \mathbf{C}_{\mathrm{m}}\left\{\mathbf{I} - k_{\mathrm{f}}\left[(\mathbf{C}_{\mathrm{f}} - \mathbf{C}_{\mathrm{m}})(\mathbf{S}^{\mathrm{E}} - k_{\mathrm{f}}(\mathbf{S}^{\mathrm{E}} - \mathbf{I}) + \mathbf{C}_{\mathrm{m}})\right]^{-1}(\mathbf{C}_{\mathrm{f}} - \mathbf{C}_{\mathrm{m}})\right\}^{-1} \tag{24}$$

where $\mathbf{I}$ is the fourth order identity tensor.

3.2.3. Comparison of results

Taken into account the results obtained with the finite element analysis described in Section 3.2.1, the lamina is considered as a composite formed by two subcomposites named *a* and *b*, which in turn, are formed by fiber and matrix. Each subcomposite *a* and *b* uses a combination tensor $\boldsymbol{\alpha}_a^{\sigma}$ and a combination tensor $\boldsymbol{\alpha}_b^{\sigma}$, respectively. Then, these subcomposites are combined between them by means of the tensor $\boldsymbol{\alpha}^{\boldsymbol{\sigma}}$.

Comparisons of the results obtained using the finite element model, the Mori–Tanaka method and the methodology presented in this paper were carried out. The objective of these comparisons was to determine the components of tensors $\boldsymbol{\alpha}^{\sigma}, \boldsymbol{\alpha}_a^{\sigma}$ and $\boldsymbol{\alpha}_b^{\sigma}$, that produce the best approximation to the behavior of an unidirectional fiber reinforced lamina. Although several combinations of subcomposites were analyzed, only the cases for which the best agreement with the results of the other described methods was achieved, are presented. Comparisons with experimental results were also performed for those cases in which this information was available. Additionally, comparisons with results obtained using the expressions proposed by Huang (2001) are included in some cases.

In all cases the best prediction of the elastic properties corresponds to the following combination: Diag $\boldsymbol{\alpha}^{\sigma} = [100000]$, Diag $\boldsymbol{\alpha}_a^{\sigma} = [111000]$, Diag $\boldsymbol{\alpha}_b^{\sigma} = [100011]$, where Diag $\boldsymbol{\alpha}^{\boldsymbol{\sigma}} = [\boldsymbol{\alpha}_{1111}, \boldsymbol{\alpha}_{2222}, \boldsymbol{\alpha}_{3333}, \boldsymbol{\alpha}_{2323}, \boldsymbol{\alpha}_{1313}, \boldsymbol{\alpha}_{1212}]$ and the volume fraction of each subcomposite are $k_a = k_b = 0.5$, the actual fiber-volume ratio is used inside each subcomponent.

Figs. 6–17 show the variation of the effective elastic properties of unidirectional laminae with respect to the

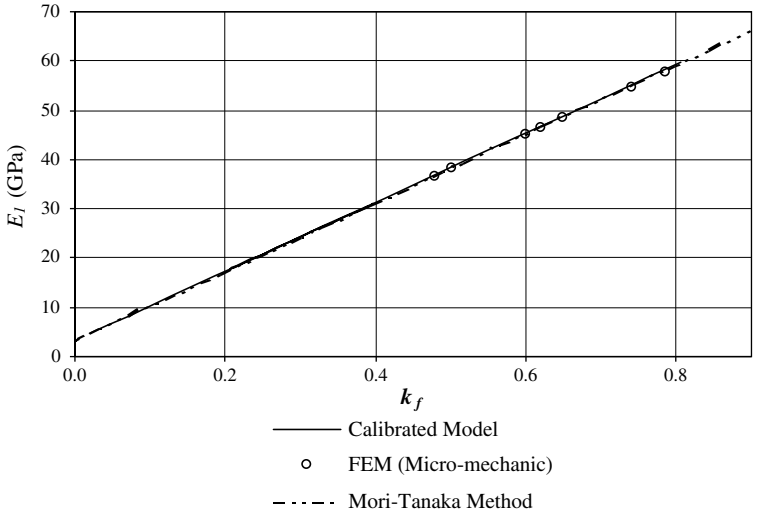

Fig. 6. Variation of E_1 with fiber-volume fraction (isotropic fiber).

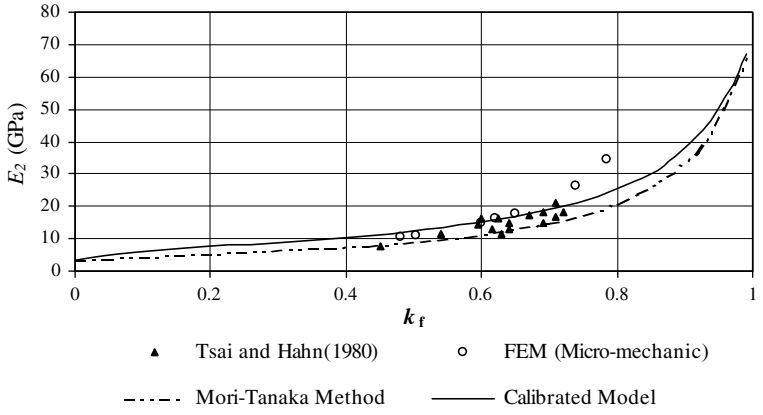

Fig. 7. Variation of E_2 with fiber-volume fraction (isotropic fiber).

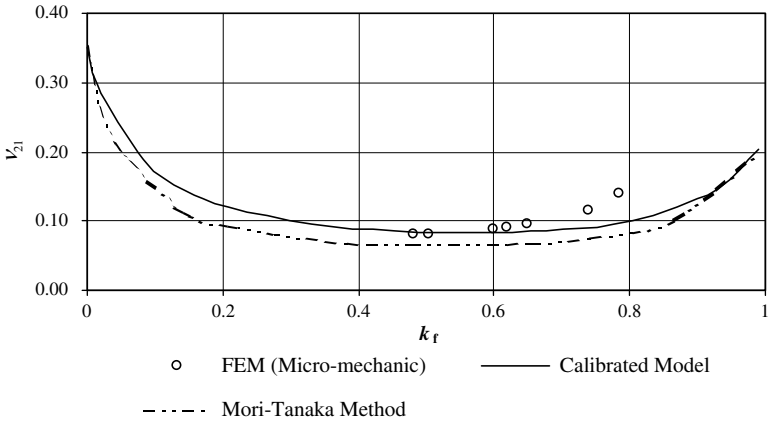

Fig. 8. Variation of v_{21} with fiber-volume fraction (isotropic fiber).

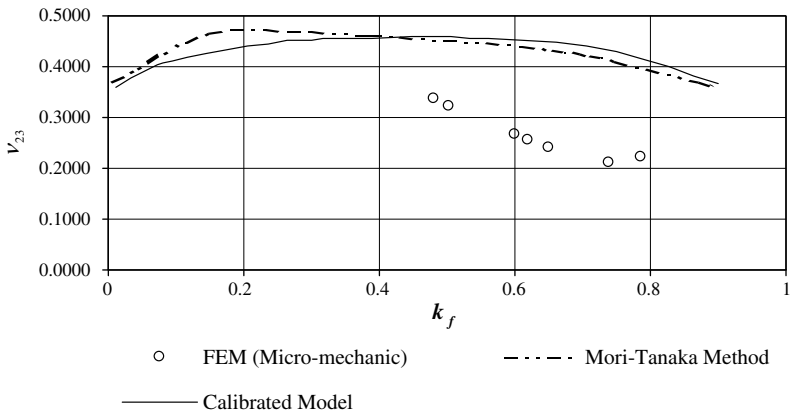

Fig. 9. Variation of v_{23} with fiber-volume fraction (isotropic fiber).

fiber-volume fraction (k_f). Figs. 6–11 also show the results corresponding to the lamina with isotropic fiber identified as Lamina 1 in Table 1. The comparison with the experimental results by Tsai and Hahn (1980) is also included in Fig. 7. On the other hand, results obtained for the lamina with orthotropic fiber identified as Lamina 2 in Table 1 are presented in Figs. 12–17 and compared with the experimental results by Kriz and Stinchcomb (1979).

Additionally, the variation of the scaled longitudinal shear modulus G_{12}/G_m (composite shear modulus/matrix

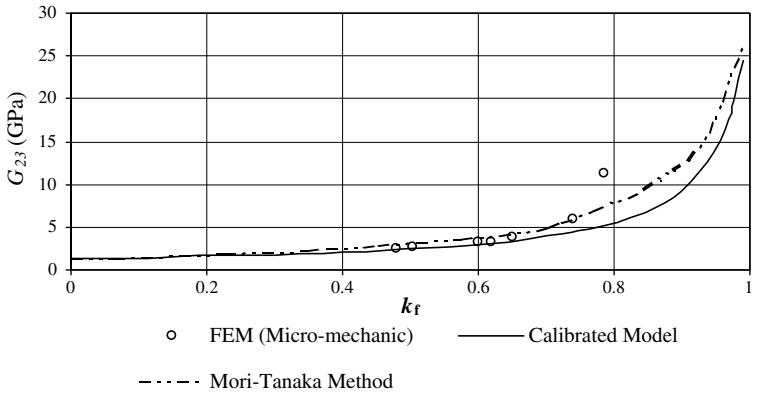

Fig. 10. Variation of G_{23} with fiber-volume fraction (isotropic fiber).

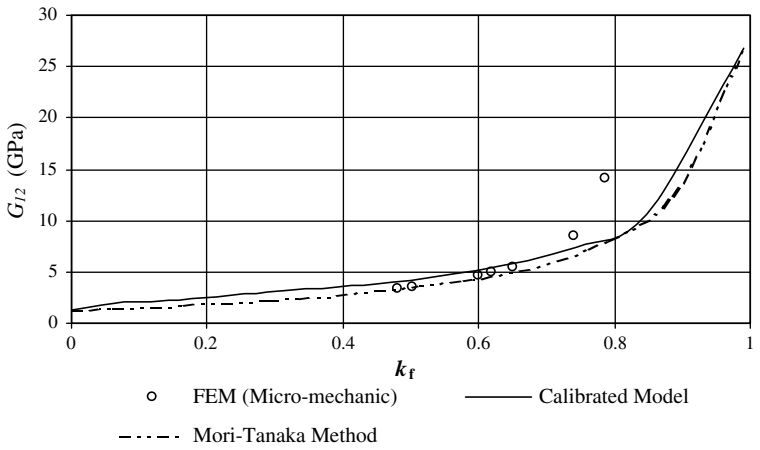

Fig. 11. Variation of G_{12} with fiber-volume fraction (isotropic fiber).

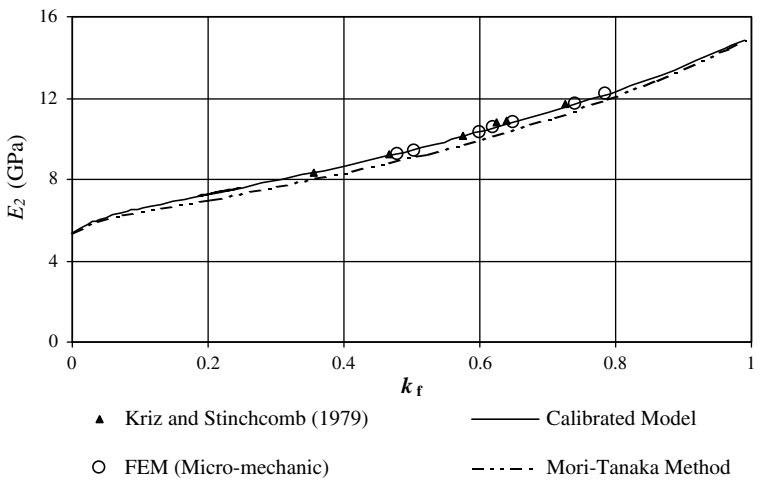

Fig. 12. Variation of E_2 with fiber-volume fraction (orthotropic fiber).

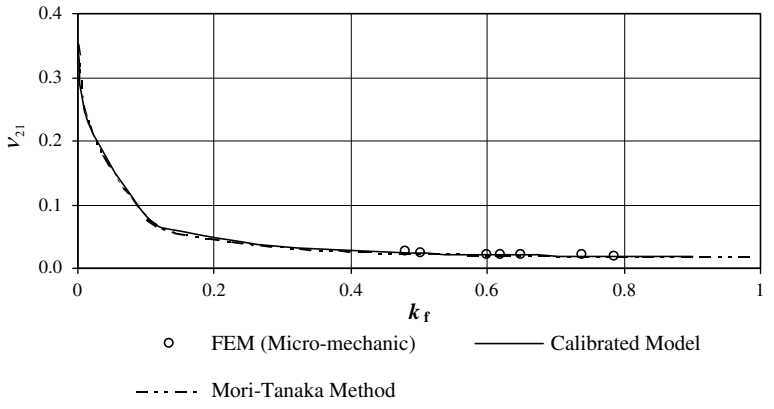

Fig. 13. Variation of v_{21} with fiber-volume fraction (orthotropic fiber).

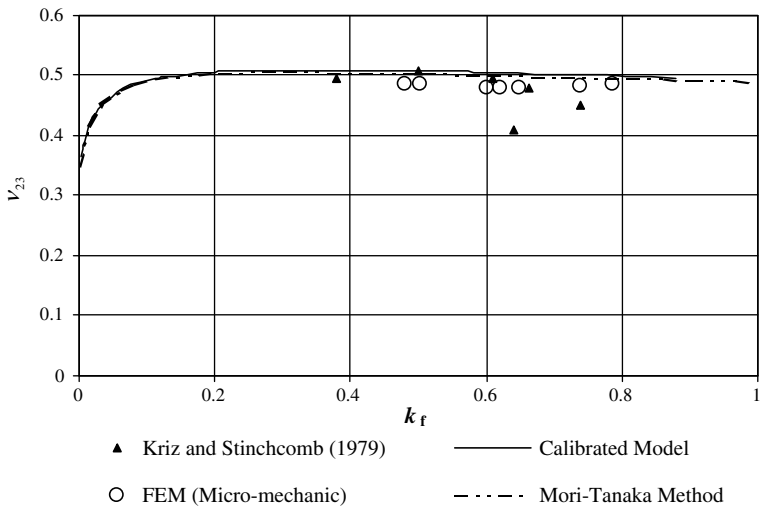

Fig. 14. Variation of v_{23} with fiber-volume fraction (orthotropic fiber).

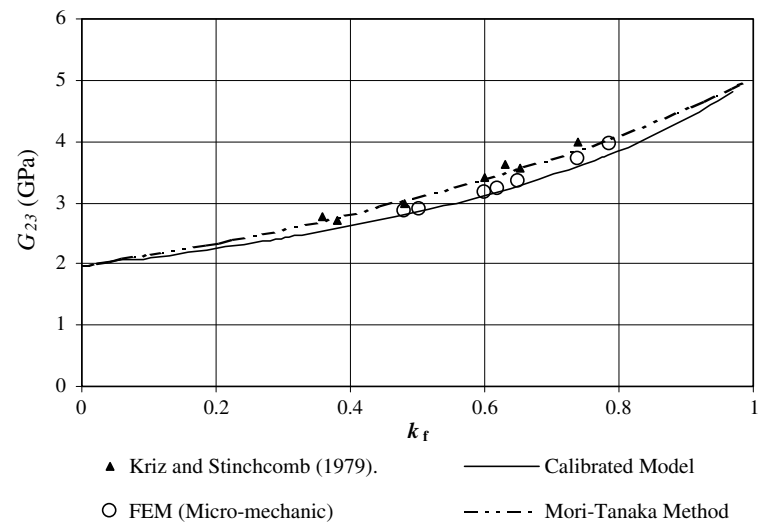

Fig. 15. Variation of G_{23} with fiber-volume fraction (orthotropic fiber).

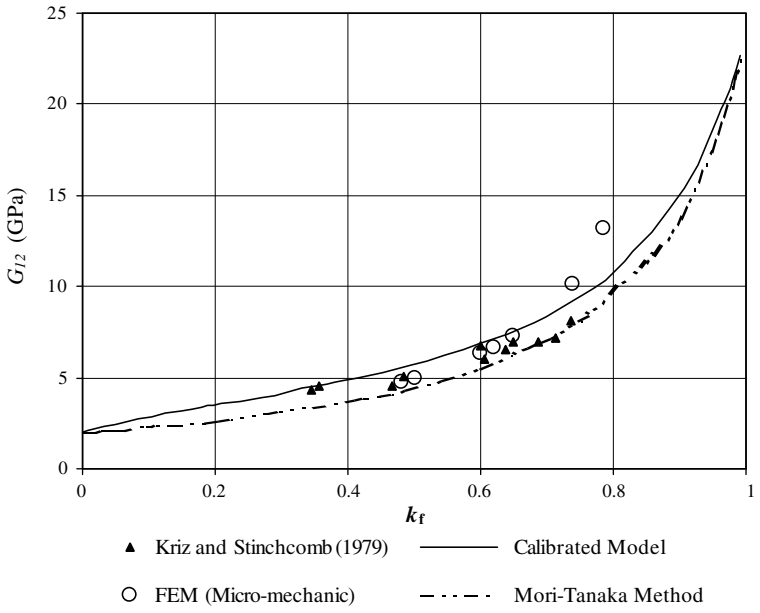

Fig. 16. Variation of G_{12} with fiber-volume fraction (orthotropic fiber).

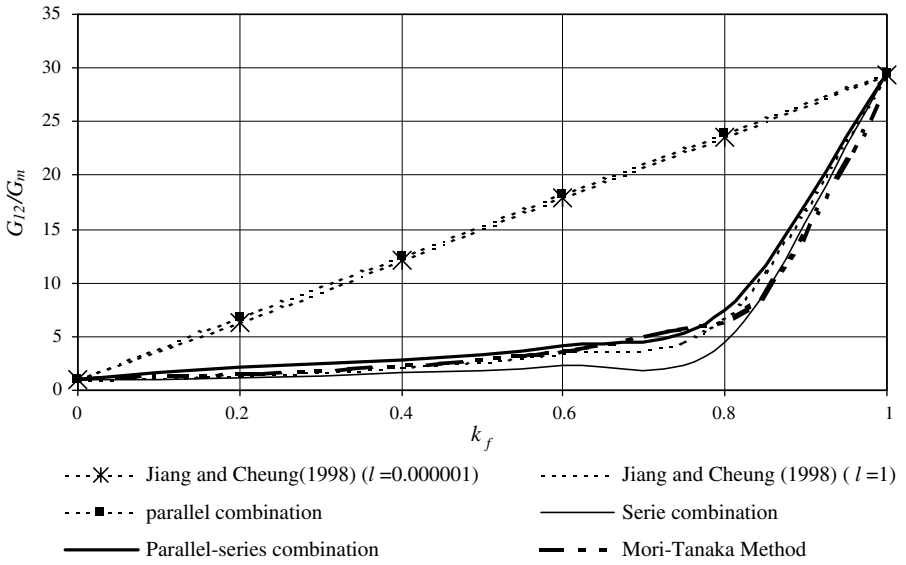

Fig. 17. Variation of G_{12} with fiber-volume fraction.

shear modulus) with the fiber-volume fraction is presented in Fig. 17. These results correspond to a composite made up with resin epoxy (Jiang and Cheung, 1998) and glass fibers with different shapes of section identified with number 7 in Table 1. Fig. 17 presents the results obtained with the proposed model considering different behaviors, i.e. series, parallel and a series combination of two subcomposites, one in series and the other one in parallel, in correspondence with the shear component 1–2. Results obtained by Jiang and Cheung (1998) using a model of elliptical elastic inclusions for various fiber section aspect ratio (the ratio of the semiminor axis to semimajor axis), l, are also presented in this figure. It is observed that the consideration of parallel behavior gives similar results to those of low aspect ratio ($l = 0.000001$), while a parallel/series combination produces a better approximation to the case of fibers with circular section ($l = 1$). This example shows that the particular combination used strongly depends on fibers cross section shape.

Taken into account that the experimental data provided by Soden et al. (1998a) in the failure exercise constitutes a very important reference point, a final comparison of this information with the elastic properties was carried out.

Table 2
Comparison of elastic properties of laminae obtained by different methods

Elastic properties	Lamina 3 (k_f = 0.6)				Lamina 4 (k_f = 0.60)			
	[1]	[2]	[3]	[4]	[1]	[2]	[3]	[4]
E_1 (GPa)	126	136.7	135.8	136.7	138	139.66	138.7	139.6
E_2 (GPa)	11	9.37	9.51	8.75	11	9.21	9.39	8.57
G_{12} (GPa)	6.6	5.01	4.66	4.14	5.50	4.83	4.47	3.98
v_{12}	0.280	0.248	0.257	0.253	0.280	0.252	0.261	0.257
v_{23}	0.4	0.284	0.261	0.319	0.4	0.299	0.272	0.336
	Lamina 5 (k_f = 0.62)				Lamina 6(k_f = 0.60)			
E_1 (GPa)	53.5	50.94	50.6	50.89	45.6	45.81	45.5	45.76
E_2 (GPa)	17.7	15.64	16.1	11.7	16.2	14.73	14.8	11.02
G_{12} (GPa)	5.83	5.37	4.9	4.61	5.83	5.07	4.53	4.32
v_{12}	0.278	0.232	0.255	0.249	0.278	0.234	0.257	0.252
v_{23}	0.4	0.455	0.252	0.440	0.4	0.453	0.265	0.440

[1] Exper. (Soden et al., 1998a) [2] Calibrated model [3] FEM (micro-mechanic) [4] Mori–Tanaka method.

Using the same combinations of the above mentioned cases, the elastic properties of the laminae identified as 3, 4, 5 and 6 in Table 1 were determined with the mentioned methods and compared with the experimental ones in Table 2.

In general, a good agreement between the model results and the experimental ones (Soden et al., 1998a) is observed. The main differences appear transversally to the fibers direction and, specially, in the Poisson ratio v_{23}. However, it is important to note that the results obtained by means of the other methods, i.e. finite elements and Mori–Tanaka cannot reproduce these experimental values either. The observed differences can be partly attributed to the lack of precision in the mechanical properties of the components, fundamentally of the fibers used as departure data. Since the fibers have very small diameters and they are difficult to handle, the determination of the mechanical properties of the fibers is not always direct. Generally, tests are carried out on unidirectional laminae, and micro-mechanical relationships are used to extract the properties of the fibers starting from the results of laminae. In consequence, it is feasible to find variability and inaccuracy in the results.

3.3. Composite laminates

3.3.1. Introduction

To apply the constitutive model described in Section 2 to a laminate, the behavior of laminae must be firstly obtained and then the behavior of laminates can be simulated, considering how the stresses and strains are transmitted among plies. For this reason, the finite element analysis carried out in this section considers two scales: a micro-mechanical scale meshing fibers and matrix of each lamina of the laminate and a meso-mechanical scale considering each lamina as homogeneous and orthotropic, with the elastic properties obtained in previous sections. As in the case of an unidirectional lamina, the micro-mechanical elastic analysis does not include the interface. The behavior of interfaces is strongly non-linear and their elastic deformations can be neglected. Similarly, when a meso-mechanical study composing laminae is carried out, the laminae interfaces are not explicitly considered. These simplifications are only made in this first calibration stage of the model in elastic regimen. Later, inelastic effects of interfaces can be included considering additional inelastic deformations in the constitutive equations of fibers and laminae (Luccioni and López, 2002) to simulate fibers debonding and delamination.

3.3.2. Finite elements model

The finite element analysis was performed with SAP 2000 Advanced 9.0.3, and three-dimensional solids elements were used (CSI Analysis Reference Manual, 2004).

Fig. 18 shows the models corresponding to the micro-mechanical scale and to the meso-mechanical scale of a composite laminate. x and y directions are contained in the laminate plane and z is normal to this plane. Each lamina can exhibit a different fiber orientation and it is defined by the angle θ formed between the principal direction 1 of the lamina and x axis.

The laminates studied in this section are the following (Soden et al., 1998a):

1. $(0°/90°)_s$ Laminate (Silenka E-glass 1200 tex, matrix MY750/HY917/DY063). The total thickness of the laminate is 1.04 mm and each play has a thickness of 0.26 mm.
2. $(\pm 45°)_s$ Laminate (Silenka E-Glass 1200 tex MY750/HY917/DY063 epoxy). The total thickness of the laminate is 1 mm and each play has a thickness of 0.25 mm.
3. $(\pm 55°)_s$ Laminate (Silenka E-Glass 1200 tex MY750/HY917/DY063 epoxy). The total thickness of the laminate is 1 mm and all the laminae have the same thickness.
4. $(90°/\pm 30°)_s$ Laminate (E-Glass/LY556/HT907/DY063). The total thickness of the laminate is 2 mm, the thickness of the ±30° plies represent 82.8% of the total thickness and laminae at 90° represent the remaining 17.2%.
5. (90°/ ± 45°/0°)s Laminate (AS4/3501–6). The total thickness of the laminate is 1.1 mm and all the laminae have the same thickness.

3.3.3. Results and model calibration

The results obtained by the micro-mechanical and the meso-mechanical analysis previously described and their comparison with the results obtained with the calibrated

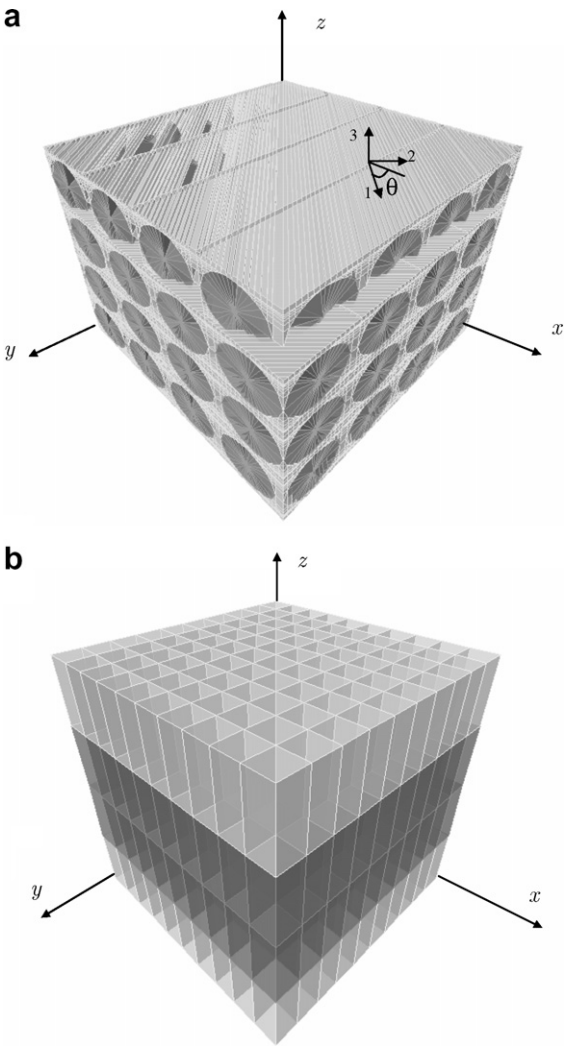

Fig. 18. Finite element mesh for: (a) micro-mechanical scale; (b) meso-mechanical scale.

model are presented in this section. In the meso-mechanical analysis, the laminae were modeled using two different approaches. On one hand, experimental data of fiber and matrix (Tables 3,4 rows (2), (3), (5); Tables 5–7, rows (2), (4) were used as input, and on the other hand, the mechanical properties of the laminae obtained from experimental tests (Tables 3, 4, rows (1) and (4); Tables 5–7, rows (1) and (2) were used.

This analysis showed that the model described in Section 2 can be used with a double combination to produce a close approximation to the experimental observed behavior. The combination is characterized by two sub-laminates obtained with Diag $\alpha_a^\sigma = [111000]$, Diag $\alpha_b^\sigma = [100011]$ and $k_a = k_b = 0.5$. In turn, each lamina of the laminate is composed using the fiber–matrix combinations previously suggested. Tables 3–7 show the elastic properties obtained using these combinations for various laminates. It can be observed that the use of the calibrated model leads to similar results to those obtained with the other approaches.

4. Application examples and comparison with experimental results

4.1. Introduction

The model described in Section 2 was implemented in a 3D non-linear finite element code and orthotropic elasto-plastic models for the components were adopted. Application examples and comparison with experimental results obtained with this code are presented in this section. Two groups of application examples are presented. The first one corresponds to the failure exercise previously mentioned (Soden et al., 1998a, 2002). The second group includes application examples concerning the tension test of an open hole coupon and comparison with experimental results by Sihn et al. (2007).

4.2. Failure exercise (Soden et al., 1998a, 2002)

All the laminates studied are formed by laminae composed of a soft matrix with continuous unidirectional fibers. The mechanical properties of the four types of epoxy resins and the four types of glass and carbon fibers are presented in Tables 8 and 9 respectively. Mohr Coulomb yield criterion was used for the matrix and an inverted Durcker Prager criterion, with less yielding threshold in compression than in tension, was used for the fibers to approximately take into account the reduction of compression strength due to fiber buckling. As there was no experimental data available defining hardening or softening behavior of matrix and fibers, the corresponding parameters were calibrated in order to properly reproduce

Table 3
Comparison of elastic properties of $(0°/90°)_s$ Laminate (Silenka E-glass 1200 tex, matrix MY750/HY917/DY063)

Model	Starting data	E_x (GPa)	ν_{xy}	ν_{xz}	E_y (Gpa)	ν_{yx}	ν_{yz}	E_z (GPa)	ν_{zx}	ν_{zy}	G_{yz} (GPa)	G_{xz} (GPa)	G_{xy} (GPa)
FEM model (meso-mech.)	Laminae	31.1	0.15	0.36	31.1	0.15	0.36	17.2	0.2	0.2	5.8	5.8	5.83
	Fiber and matrix	30.3	0.13	0.27	30.3	0.13	0.27	15.1	0.14	0.14	4.91	4.91	4.53
FEM model (micro-mech.)	Fiber and matrix	29.2	0.12	0.28	29.2	0.12	0.28	14.7	0.13	0.13	4.27	4.27	4.41
Calibrated model (meso-mech.)	Laminae	31.1	0.15	0.36	31.1	0.15	0.36	17.2	0.2	0.2	5.81	5.81	5.83
Calibrated model (micro-mech.)	Fiber and matrix	30.3	0.13	0.27	30.3	0.13	0.27	15.1	0.14	0.14	5.19	5.19	4.53

Table 4
Comparison of elastic properties of $(\pm 45°)_s$ Laminate (Silenka E-Glass 1200 tex MY750/HY917/DY063 epoxy)

Model	Starting data	E_x (GPa)	v_{xy}	v_{xz}	E_y (Gpa)	v_{yx}	v_{yz}	E_z (GPa)	v_{zx}	v_{zy}	G_{yz} (GPa)	G_{xz} (GPa)	G_{xy} (GPa)
FEM model (meso-mech.)	Laminae	17.6	0.51	0.21	17.6	0.51	0.21	17.9	0.21	0.21	5.6	5.6	11.3
	Fiber and matrix	14.3	0.58	0.13	14.3	0.58	0.13	15.7	0.14	0.14	4.72	5.16	10.8
FEM model (micro-mech.)	Fiber and matrix	17.0	0.44	0.21	17.1	0.41	0.23	14.3	0.13	0.13	4.26	4.85	10.6
Calibrated model (meso-mech.)	Laminae	17.7	0.51	0.2	17.7	0.52	0.2	17.2	0.2	0.2	5.81	5.81	12.0
Calibrated model (micro-mech.)	Fiber and matrix	14.4	0.59	0.13	14.4	0.59	0.13	15.1	0.14	0.14	5.19	5.19	11.7

Table 5
Comparison of elastic properties of $(\pm 55°)_s$ Laminate (Silenka E-Glass 1200 tex MY750/HY917/DY063 epoxy)

Model	Starting data	E_x (GPa)	v_{xy}	v_{xz}	E_y (Gpa)	v_{yx}	v_{yz}	E_z (GPa)	v_{zx}	v_{zy}	G_{yz} (GPa)	G_{xz} (GPa)	G_{xy} (GPa)
FEM model (meso-mech.)	Laminae	15.4	0.38	0.27	23.3	0.57	0.17	17.7	0.31	0.13	5.6	5.58	12.5
	Fiber and matrix	12.7	0.42	0.17	20.2	0.66	0.12	15.6	0.21	0.09	4.72	5.16	12.2
FEM model (micro-mech.)	Laminae	15.4	0.38	0.27	23.5	0.58	0.17	17.0	0.3	0.12	5.81	5.80	11.1
Calibrated model (micro-mech.)	Fiber and matrix	12.7	0.42	0.17	20.4	0.67	0.11	15.1	0.21	0.08	4.96	5.42	10.6

Table 6
Comparison of elastic properties of $(90°/\pm 30°)_s$ Laminate (E-Glass/LY556/HT907/DY063)

Model	Starting data	E_x (GPa)	v_{xy}	v_{xz}	E_y (Gpa)	v_{yx}	v_{yz}	E_z (GPa)	v_{zx}	v_{zy}	G_{yz} (GPa)	G_{xz} (GPa)	G_{xy} (GPa)
FEM model (meso-mech.)	Laminae	29.5	0.40	0.23	22.3	0.32	0.31	18.7	0.15	0.24	6.15	6.03	10.9
	Fiber and matrix	26.9	0.41	0.18	20.2	0.33	0.2	16.4	0.11	0.16	5.79	5.42	10.0
Calibrated model (meso-mech.)	Laminae	29.9	0.43	0.23	22.3	0.32	0.29	18.8	0.15	0.24	6.14	6.02	10.2
Calibrated model (micro-mech.)	Fiber and matrix	27.4	0.42	0.18	20.2	0.33	0.2	16.4	0.11	0.16	5.85	5.48	9.29

Table 7
Comparison of elastic properties of $(90°/\pm 45°/0°)$s Laminate (AS4/3501–6)

Model	Starting data	E_x (GPa)	v_{xy}	v_{xz}	E_y (Gpa)	v_{yx}	v_{yz}	E_z (GPa)	v_{zx}	v_{zy}	G_{yz} (GPa)	G_{xz} (GPa)	G_{xy} (GPa)
FEM model (meso-mech.)	Laminae	49.6	0.25	0.3	49.6	0.25	0.3	12.5	0.08	0.08	4.94	4.94	17.1
	Fiber and matrix	50.4	0.26	0.22	50.4	0.26	0.22	10.0	0.04	0.04	4.15	4.15	16.5
Calibrated model (meso-mech.)	Laminae	51.1	0.29	0.28	51.1	0.29	0.29	12.6	0.07	0.07	5.26	5.26	13.8
Calibrated model (micro-mech.)	Fiber and matrix	52.2	0.31	0.21	52.2	0.31	0.21	10.1	0.04	0.04	4.22	4.22	13.0

the behavior of the lamina and were also included in Tables 8 and 9. Then, the same parameters were used to combine laminae in a laminate.

Almost all experimental results used were derived from tests on tube specimens. Numerical results were all obtained for a 100 mm × 100 mm model with the lamina or laminate thickness and a three-dimensional analysis was performed. The use of these models is justified by the fact that in tube specimens a global plane stress state for the lamina or the laminate is obtained. Tetrahedral elements with 4 nodes and 3 degrees of freedom for node were used. Fig. 19 shows the finite element mesh used in all cases.

4.2.1. Laminae

In general, structures are not designed with all the fibers aligned in a unique direction if the structure is

Table 8
Matrices mechanical properties (Soden et al., 1998a)

Matrix	3501-6 epoxy	BSL914C epoxy	LY556/HT907/DY063 epoxy	MY750/HY917/DY063 epoxy
Tension strength, Y_{mt} (MPa)	69	75	80	80
Compres. strength, X_{mc} (MPa)	250	150	120	120
Shear strength, S_m (MPa)	50	70	–	–
Ultimate tension strain, ε_{mt} (%)	1.7	4	5	5
Compression hardening function ([a])	Exponential with peak non-linear limit 180 MPa peak position 0.25 of total plastic work	Exponential with peak non-linear limit 100 MPa peak position 0.15 of total plastic work	Exponential with peak non-linear limit 100 MPa peak position 0.2 of total plastic work	Exponential with peak non-linear limit 100 MPa peak position 0.20 of total plastic work
Tension hardening function	Exponential decay	Exponential decay	Exponential decay	Exponential decay

[a] Data obtained from calibration.

Table 9
Fibers mechanical properties (Soden et al., 1998a)

Fiber	AS4	T300	E-Glass 21 × 43 Gevetex	Silenka E-Glass 1200 tex
Long. tensile strength, X_{ft} (MPa)	3350	2500	2150	2150
Long. compres. strength, X_{fc} (MPa)	2500	2000	1450	1450
Ultimate tensile strain, ε_{f1T} (%)	1.488	1.086	2.687	2.905
Ultimate compres. strain, ε_{f1c} (%)	1.111	0.869	1.813	1.959
Slope of linear compression hardening function (MPa)([a])	0.0	20	5	5
Slope of tension hardening function (MPa) ([a])	0.0	20	5	5

[a] Data obtained from calibration.

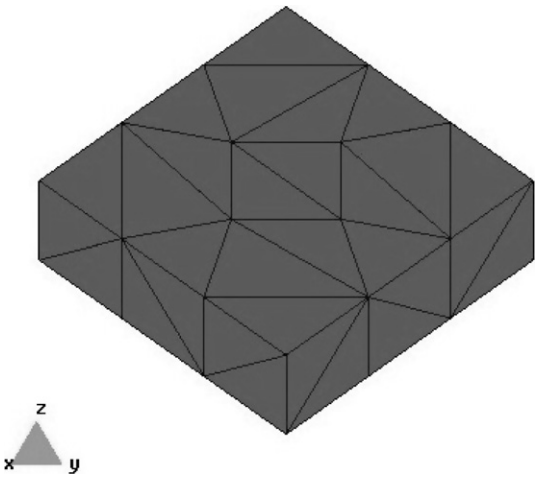

Fig. 19. Finite element mesh.

expected to be exposed to stresses in the orthogonal direction. However, unidirectional laminae constitute the basic elements of the laminate and, inside it, they can be subjected to stresses normal to the fiber direction and shear stresses. So, it is important to know first of all, if the models are able to reproduce the behavior of an individual lamina.

4.2.1.1. Lamina 3 (AS4/3501–6). The non-linear in plane behavior of a lamina reinforced with carbon fiber (AS4) and epoxy matrix 3501-6 (Soden et al., 1998a) is studied in this section. Fig. 20 shows the stress–axial strain and the stress–transversal strain curves in tension test in fibers direction. The behavior is almost linear up to the brittle failure of the fibers in tension. A good agreement between numerical and experimental results can be observed. There are more pronounced differences in transversal strains, which are defined by the Poisson ratio.

The behavior of the lamina under compression normal to the fiber orientation is shown in Fig. 21. The curves represent the stress–strain response in the load direction and in the transverse direction. A reasonable agreement of the numerical results with the experimental ones is obtained. A non-linear behavior from lower stresses due to matrix crushing is observed in this case.

Finally, the shear stress–shear strain curve for a pure shear test is presented in Fig. 22. In this case the numerical model also reproduces the experimental results properly. The non-linearity in the behavior is first due to the shear failure of the matrix followed by the fibers shear failure.

4.2.1.2. Lamina 4 (T300/BSL914C epoxy). The non-linear in plane behavior of a lamina reinforced with carbon fibers T300 and epoxy matrix BSL914C is analyzed in this point. The shear stress–angular strain curve for a pure shear test is plotted in Fig. 23. A good agreement with experimental results is also achieved in this case.

4.2.1.3. Lamina 5 (E-Glass/LY556 epoxy). The non-linear in plane behavior of a lamina reinforced with glass fibers and epoxy matrix LY556 is studied in this point. Fig. 24 shows the shear stress–angular strain for a pure shear test. A good agreement between numerical and experimental results (Soden et al., 1998a) is obtained. The non-linear behavior is analogous to that observed in Lamina No. 4.

4.2.1.4. Lamina 6 (Silenka E-Glass 1200 tex MY750/HY917/DY063 epoxy). The non-linear in plane behavior of a lamina reinforced with glass fibers Silenka E-Glass 1200 tex and epoxy matrix 3501-6 MY750/HY917/DY063 is studied in this point. The stress–strain curve in the load direction and the stress–strain in the transverse direction when the lamina is subjected to compression perpendicular to the fiber direction is presented in Fig. 25. A reasonable

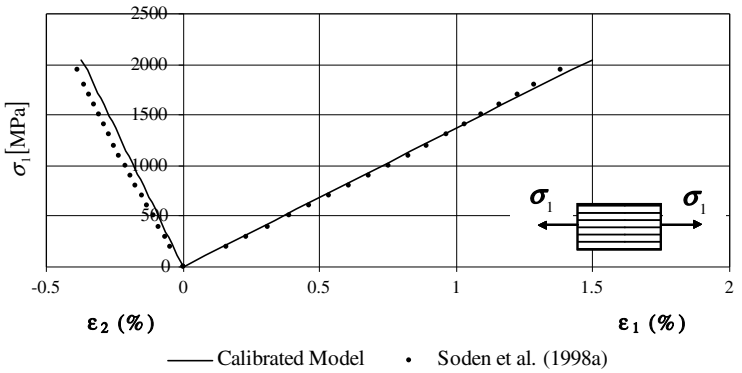

Fig. 20. Longitudinal tensile stress/strain curve for Lamina 3 (AS4/3501–6).

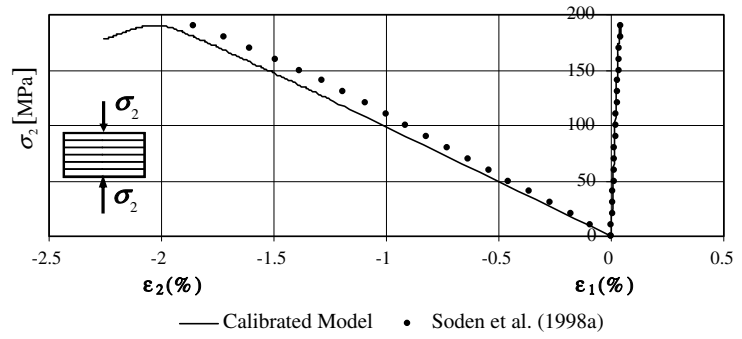

Fig. 21. Transverse compressive stress/strain curve for Lamina 3(AS4/3501-6).

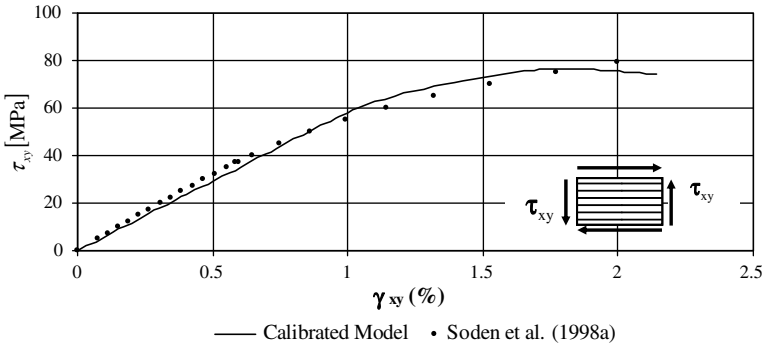

Fig. 22. In-plane shear stress/strain curve for Lamina 3(AS4/3501-6).

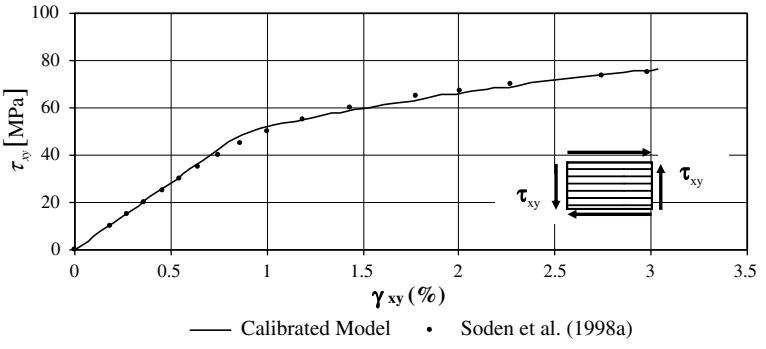

Fig. 23. In-plane shear stress/strain curve for Lamina 4 (T300/BSL914C epoxy).

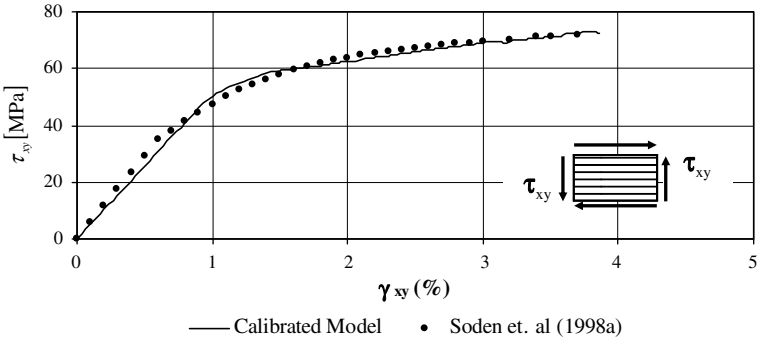

Fig. 24. In-plane shear stress/strain curve for Lamina 5 (E-Glass/LY556 epoxy).

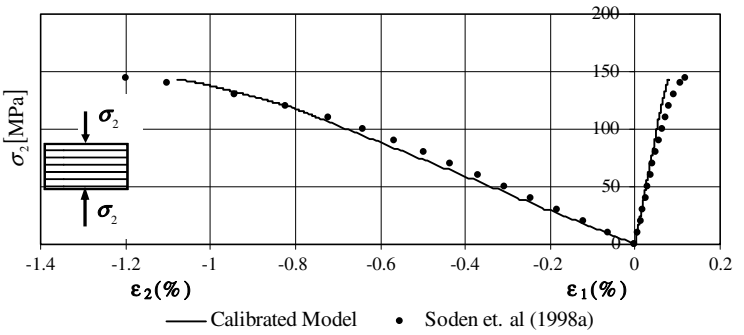

Fig. 25. Transverse compressive stress/strain curve for Lamina 6 (Silenka E-Glass 1200 tex MY750/HY917/DY063 epoxy).

agreement with experimental results (Soden et al., 1998a) can be observed. A non-linear behavior from lower stresses is obtained due to the matrix crushing.

The shear stress–angular strain curve in a pure shear test is plotted in Fig. 26. A reasonable agreement with the experimental results is observed. The non-linear behavior is first due to the matrix shear failure soon followed by the fibers shear failure.

4.2.2. Laminates

In this section the non-linear response of the laminates described in Section 3 is analyzed.

4.2.2.1. $(0°/90°)_s$ Laminate (Silenka E-glass 1200 tex, matrix MY750/HY917/DY063). The typical stress–strain experimental curves obtained in uniaxial tension tests (Soden et al., 2002) are shown in Fig. 27. The onset of the first crack was recorded at a strain of $\varepsilon_y = 0.375\%$, which corresponds to a load per unit area 117.5 MP on the coupon. The onset of longitudinal splitting was observed at a strain of $\varepsilon_y = 1.3\%$. The coupons finally failed by fiber fracture.

The stress–strain curves obtained with the calibrated model under uniaxial tension $\sigma_y{:}\sigma_x = 1{:}0$ are plotted in Fig. 27 together with the experimental results described above. Numerical results properly reproduce the experimentally observed behavior.

4.2.2.2. $(\pm 45°)_s$ Laminate (Silenka E-Glass 1200 tex MY750/HY917/DY063 epoxy). The specimens used for the tests (Soden et al., 2002) were in the form of (±45°) tubes. They were 100 mm inner diameter, 310 mm overall length, 60 mm gauge length and typically 1 mm thick. The tubes

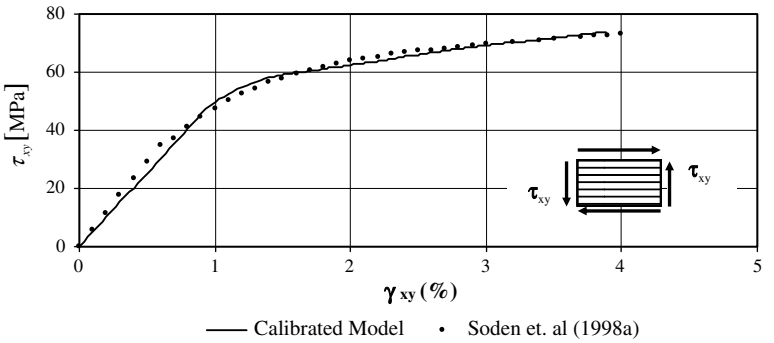

Fig. 26. In-plane shear stress/strain curve for Lamina 6 (Silenka E-Glass 1200 tex MY750/HY917/DY063 epoxy).

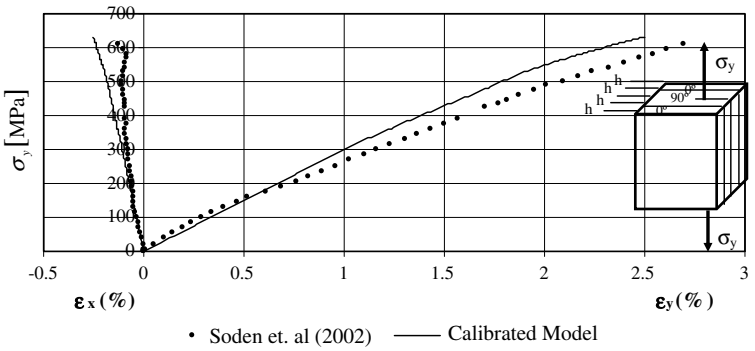

Fig. 27. Stress–strain curves for $(0°/90°)_s$ Laminate (Silenka E-glass 1200 tex, matrix MY750/HY917/DY063) under uniaxial tensile loading with $\sigma_y:\sigma_x = 1:0$.

were reinforced at the ends and tested under internal pressure and axial load, obtaining equal biaxial tension states ($\sigma_y:\sigma_x = 1:1$).

One of the peculiar features of these experimental results is that the hoop strains are larger than the axial strains, although ideally they should be equal to each other. Reasons for such divergence are not clear (Soden et al., 2002).

The specimens failed by extensive cracking parallel to the fibers, presumably due to transverse tension and by fiber tension fracture in the gauge length (Soden et al., 2002).

The stress–strain curves under biaxial tension obtained with the calibrated numerical model and the comparison with the experimental curves are shown in Fig. 28. A general coincident trend is observed, but the difference between numerical results and experimental ones is greater than in previous examples. Differences between axial and hoop strains also appear in the numerical solution. In this case, they are probably caused by numerical errors.

4.2.2.3. $(\pm 55°)_s$ Laminate (Silenka E-Glass 1200 tex MY750/HY917/DY063 epoxy). The stress–stain curves under uniaxial tension $\sigma_y:\sigma_x = 1:0$ are obtained in this section. Experimental results used for comparison purpose correspond to tests on specimens in the form of (±55°) E-glass/epoxy tubes (Soden et al., 2002). The tubes were 100 mm inner diameter, 310 mm overall length, 60 mm gauge length and typically 1 mm thick.

Fig. 29 shows the $\sigma_y - \varepsilon_y$ and $\sigma_y - \varepsilon_x$ curves obtained with the calibrated numerical model and the comparison with experimental results (Soden et al., 2002). A good agreement between numerical and experimental results is observed.

4.2.2.4. $(90°/\pm 45°/0°)_s$ Laminate (AS4/3501–6). The experimental results used in this point correspond to tests on tubes of 96.5 mm inside diameter, approximately, 1 mm thick and 419 mm total length, (Soden et al., 2002). The tubes were tested under uniaxial tension $\sigma_y:\sigma_x = 1:0$. The circumferential failure stress was 718 MPa and the hoop failure was $\varepsilon_y = 1.45\%$ and the axial strain was $\varepsilon_x = -0.36\%$.

The stress–strain curves obtained with the calibrated numerical model and the comparison with the experimental ones are presented in Fig. 30. The curves obtained with the numerical model, starting with the mechanical

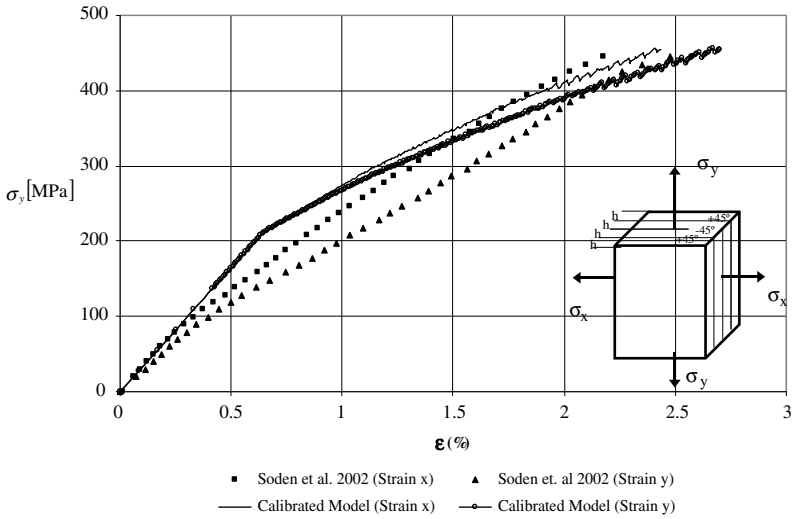

Fig. 28. Stress–strain curves for $(\pm 45°)_s$ Laminate (Silenka E-Glass 1200 tex MY750/HY917/DY063 epoxy) under biaxial tensile loading with $\sigma_y:\sigma_x = 1:1$.

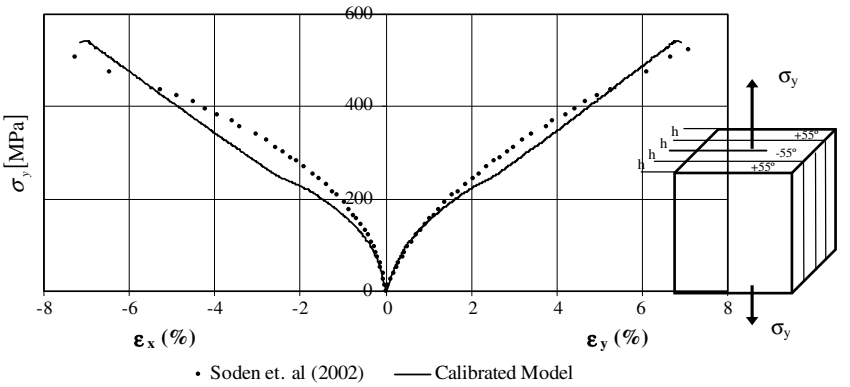

Fig. 29. Stress–strain curves for $(\pm 55^\circ)_s$ Laminate (Silenka E-Glass 1200 tex MY750/HY917/DY063 epoxy) under uniaxial tensile loading with σ_y:σ_x = 1:0.

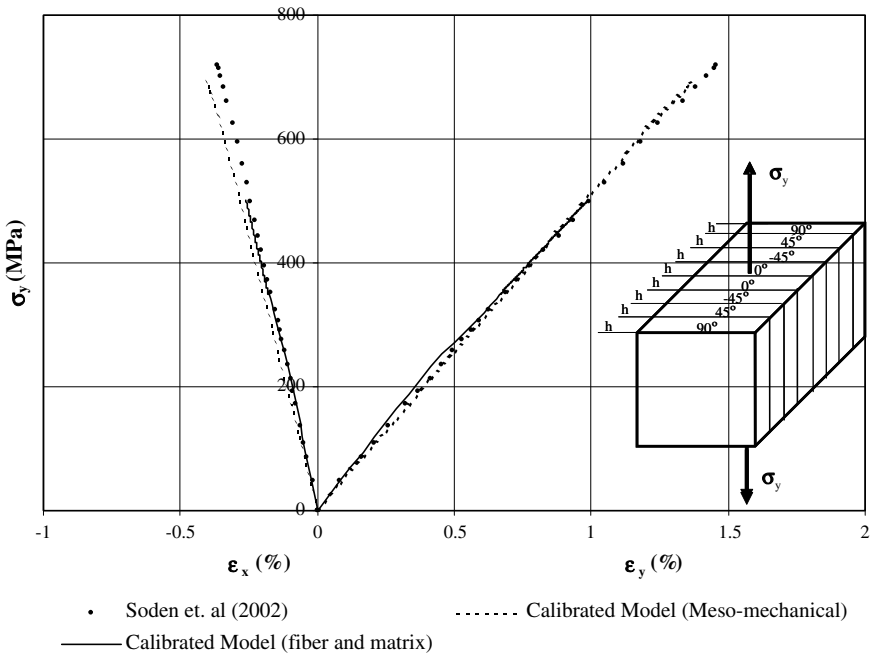

Fig. 30. Stress–strain curves for $(90^\circ/\pm 45^\circ/0^\circ)_s$ Laminate (AS4/3501–6) under uniaxial tensile loading with σ_y:σ_x = 1:0.

properties of fiber and matrix (micro-mechanical approach), and starting with those of the laminae (meso-mechanical approach) are included in Fig. 30. A good agreement with the experimental results can be observed in both cases. On the other hand, for a stress nearby to 400 MPa, the experimental curve presents a slope decrease that indicates a form of initial failure in the laminate. This effect is also reproduced by numerical results.

The stress–strain curves under biaxial tension (σ_y:σ_x = 2:1) and the comparison with the experimental results of the failure exercise (Soden et al., 2002) are shown in Fig. 31. The response is linear at low strain levels but shows a significant softening at higher strains. The non-linear behavior starts at a strain between ε_y = 0.6% and ε_y = 0.8% that corresponds to a change in the slope of stress–strain curves around σ_y = 450 MPa hoop stress. The final hoop strengths of the two tubes tested were 857 and 847 MPa. The numerical results follow the trend observed in the tests with reasonable accuracy in calculated strain values.

4.3. Tension test of an open hole coupon

Composites test specimens are made with Toray's carbon fibers (T800SC-24K) and Bryte's epoxy film resin (BT250E-1) as the fiber and matrix material in the composites, respectively (Sihn et al., 2007). The performance of two types of thin laminates was analyzed: the quasi-isotropic laminate (25/50/25) and the hard laminate (50/40/10), where three numbers in parentheses represent the percentage of the [0], [±45] and [90] plies, respectively. The mechanical properties used for the unidirectional laminae are presented in Table 10. Tresca criterion was used to model unidirectional lamina strength.

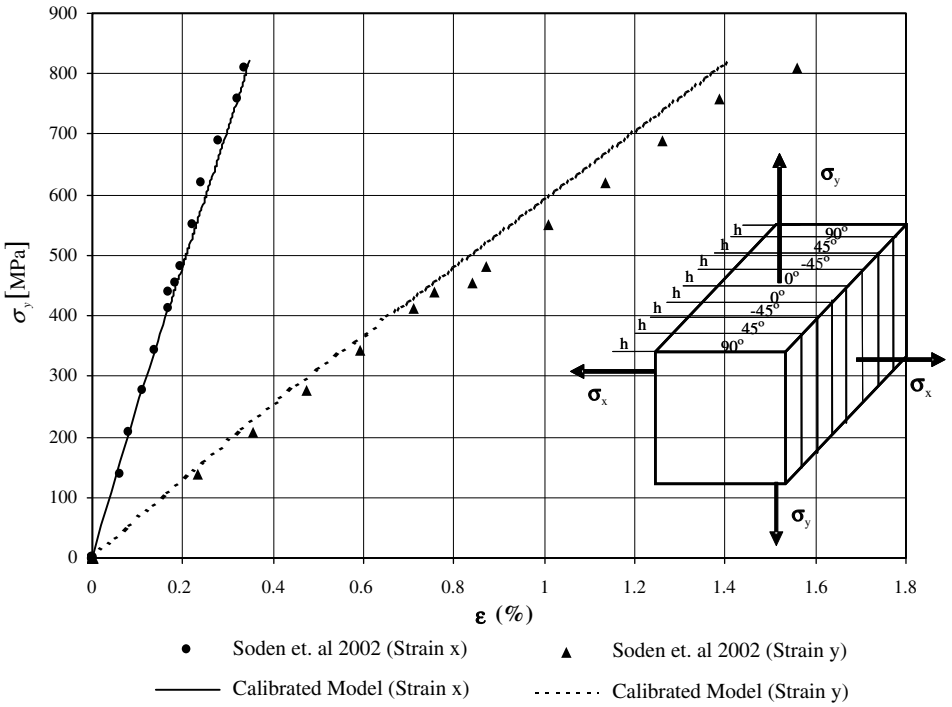

Fig. 31. Stress–strain curves for (90°/ ± 45°/0°)s Laminate (AS4/3501–6) under biaxial tensile loading with $\sigma_y : \sigma_x = 2:1$.

Table 10
Mechanical properties of laminae used in open hole tests (Sihn et al., 2007)

Fiber	Toray's carbon
Matrix	Bryte's epoxy film
Long. stiffness E_1 (GPa)	168.0
Long. stiffness E_2 (GPa)	8.4
Poisson ratio ν_{12}	0.33
Long. tensile strength, X (MPa)	2740.0
Transverse tensile strength, Y (MPa)	66.0
Tension hardening function	Exponential decay

The laminae are combined to form the laminate using Diag $\boldsymbol{\alpha}^{\boldsymbol{\sigma}} = [1\,1\,1\,0\,1\,1]$. This combination was shown to better reproduce the mechanical behavior of thin laminates.

The test considered was the open-hole tension (OHT). The width of the specimen is 38.1 mm and the diameter of the hole is 6.35 mm. Fig. 32 shows the finite element model used to simulate the tests. It represents a quarter of the central part (76.2 mm) of actual specimens. Tetrahedral elements with 4 nodes and 3 degrees of freedom for node were used.

The stress–strain curves obtained away from the hole (far field) and at a point located 1.27 mm away from the hole edge (edge) are presented in Figs. 33 and 34 for the quasi isotropic and the hard laminate respectively. Applied stress (far field) versus longitudinal strains is represented in both figures. Experimental results are also included in Figs. 33 and 34. A reasonable agreement between numerical and experimental results is obtained for both laminates. As observed in the tests, there is a stress concentration near the hole but there is no damage and stresses are not relaxed, they increased until a sudden

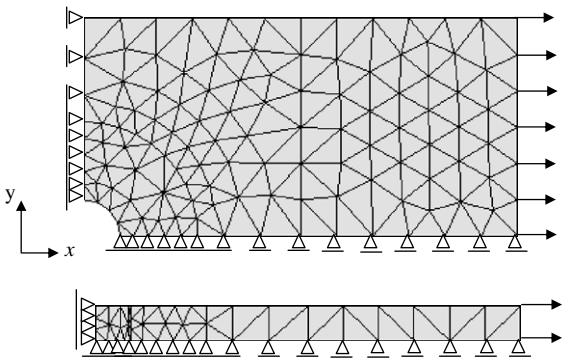

Fig. 32. Finite element mesh for the specimen under open hole tension test.

failure occurs. This observation also justifies the nearly linear strain–stress curves obtained for both laminates. As stated by Sihn et al. (2007) this behavior is due to the reduced thickness of the laminae and it can be taken into account in the numerical model with the proper definition of tensor $\boldsymbol{\alpha}^{\boldsymbol{\sigma}}$.

A similar model was used to reproduce the open hole tension tests by Tay-Earn et al. (2006). Who presented the analysis of open-hole composite laminates under uniform remote tension loading. Damage progression for a carbon–epoxy cross-ply laminate with a stacking sequence $[0_3/90_4]$s was studied. The dimension of the specimens tested by Sihn et al. (2007) is just twice those tested by Tay-Earn et al. (2006).

The same properties in Table 10 were used for the unidirectional lamina.

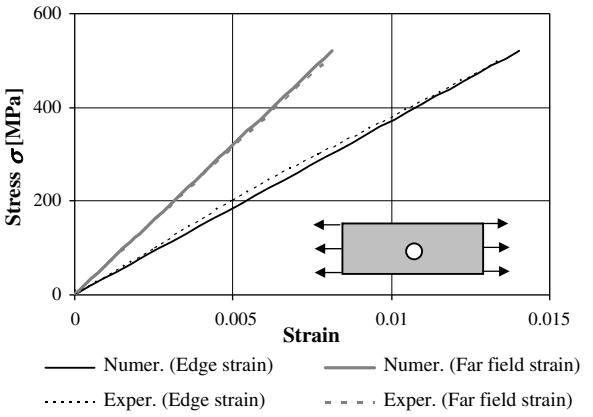

Fig. 33. Stress–strain curves for the open hole test of a quasi isotropic laminate.

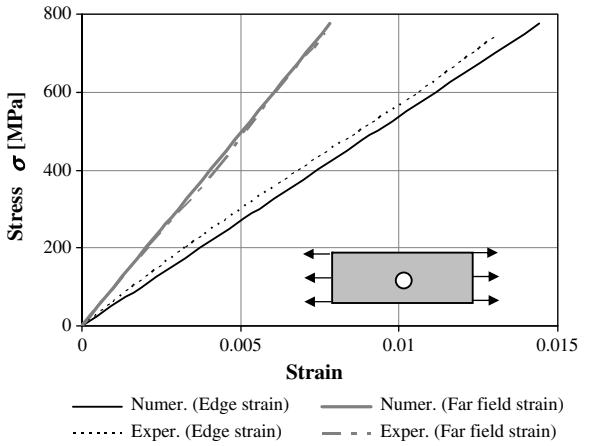

Fig. 34. Stress–strain curves for the open hole test of a hard laminate.

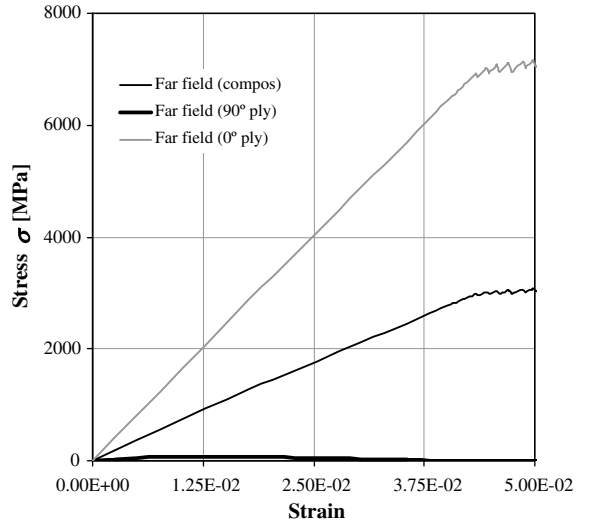

Fig. 35. Stress–strain curves for the open hole test of a $[0_3/90_4]_s$ laminate.

Far field stress–strain curves obtained for 0° ply, 90° ply and the laminate are presented in Fig. 35. Stress corresponds to the actual tensile stress in each ply or the composite. Fig. 35 shows that 90° plies damage first due to transverse matrix cracking. Damage in the 0° plies appears much later than damage in the 90° plies, since the latter are weaker. Damage in 0° ply is apparently retarded by the combination of stress generated in the lamina. These results are coincident with those presented by Tay-Earn et al. (2006).

5. Conclusions

The constitutive model presented in this paper is able to reproduce the behavior of laminated composite formed by unidirectional fiber reinforced laminae with different orientations under small strains satisfactorily.

The model was calibrated performing a detailed elastic finite element analysis and an analytical study using the Mori–Tanaka method particularized for infinite inhomogeneous cylindrical inclusions of circular section. The kinematics and equilibrium hypotheses for the calibration of the scheme model were deduced from the previously described analysis and comparisons with experimental results. The suggested hypotheses are the simplest that can be applied to isotropic fibers so as to orthotropic fibers.

A good agreement is observed among numerical and experimental results, with smaller differences in the transversal strains that are defined by the Poisson ratio; this can be due basically to the lack of precision in the mechanical properties of the components, fundamentally of the fibers, used as input data.

In general, application examples and comparison with experimental results show that the model is able to properly reproduce the mechanical behavior of laminae reinforced with unidirectional fibers and composite laminates. Better predictions were obtained in shear dominant cases. The model also describes the failure of the composite, taking into account what happens in each component. It also allows identifying the failure mode of the composite, produced by the failure of one or more of its components. It is able to reproduce complex failure modes that change from the matrix to the fibers, depending on the type of stress state. Although fiber debonding and delamination were taken into account in a simplified way, introducing a fictitious orthotropy in the components, these problems can be treated more rigorously. The inelastic deformations of the fiber–matrix and interlaminar interfaces can be introduced in the matrix and laminae constitutive models using an approach similar to that one used by Luccioni and López (2002) and Luccioni et al. (2005).

The model works better for some types of laminates and for particular load conditions The practically bi – linear curves obtained for some cases are mainly attributed to the simple curves used to define fibers and matrix hardening and show the need of further analysis and model calibration.

Two extreme cases were covered in the paper: fibers with circular cross section and elliptic fibers with very low aspect ratio. The framework presented is potentially valid for other fiber shapes but the calibration for these cases would require further development.

Acknowledgements

The authors wish to thank the economical support of CONICET, CIUNT and Facultad de Ingeniería (UNSA, BID 1728/OC-AR) and Mrs. Amelia Campos for the English revision.

References

Basu, S., Waas, M., Ambur, D., 2007. Prediction of progressive failure in multidirectional composite laminated panels. Int. J. Solids Struct. 44, 2648–2676.

Benveniste, Y., 1985. The effective mechanical behavior of composite materials with imperfect contact between the constituents. Mech. Mater. 4, 197–208.

Betten, J., 1988. Application of tensor functions to the formulation of yield criteria for anisotropic materials. Int. J. Plasticity 4, 29–46.

Bonora, N., Ruggiero, A., 2006a. Micromechanical modeling of composites with mechanical interface – Part 1: Unit cell model development and manufacturing process effects. Compos. Sci. Technol. 66, 314–322.

Bonora, N., Ruggiero, A., 2006b. Micromechanical modeling of composites with mechanical interface – Part II: Damage mechanics assessment. Compos. Sci. Technol. 66, 314–322.

Car, E., Oller, S., Oñate, E., 1999. A large strain plasticity model for anisotropic composite material application. Int. J. Plasticity 17 (11), 1437–1463.

Chaboche, J.L., Lesne, O., Pottier, T., 1998. Continuum damage mechanics of composites: towards a unified approach. Damage Mech. Eng. Mater., Stud. Appl. Mech. 46, 3–26.

CSI Analysis Reference Manual, 2004. Computers and Structures, Inc. Berkeley, California, USA.

Eshelby, J.D., 1957. The determination of the elastic field of an ellipsoidal inclusion and related problems. Proc. R. Soc. London 241, 376–396.

Hinton, M.J., Soden, P.D., 1998. Predicting failure in composite laminates: the background to the exercise. Compos. Sci. Technol. 58, 1001–1010.

Hinton, M.J., Kaddour, A.S., Soden, P.D., 2002. Evaluation of failure prediction in composite laminates: background to 'part B' of the exercise. Compos. Sci. Technol. 62, 1481–1488.

Hinton, M.J., Kaddour, A.S., Soden, P.D., 2004a. Evaluation of failure prediction in composite laminates: background to 'part C' of the exercise. Compos. Sci. Technol. 64, 321–327.

Hinton, M.J., Kaddour, A.S., Soden, P.D., 2004b. A further assessment of the predictive capabilities of current failure theories for composite laminates: comparison with experimental evidence. Compos. Sci. Technol. 64, 549–588.

Huang, Z., 2001. Micromechanical prediction of ultimate strength of transversely isotropic fibrous composites. Int. J. Solids Struct. 38, 4147–4172.

Huang, Z.M., 2007. Failure analysis of laminated structures by FEM based on nonlinear constitutive relationship. Compos. Struct. 77, 270–279.

Jiang, C.P., Cheung, Y.K., 1998. A fiber/matrix/composite model with a combined confocal elliptical cylinder unit cell for predicting effective longitudinal shear modulus. Int. J. Solids Struct. 35, 3977–3987.

Kaddour, A.S., Hinton, M.J., Soden, P.D., 2004. A comparison of the predictive capabilities of current failure theories for composite laminates: additional contributions. Compos. Sci. Technol. 64, 449–476.

Knops, M., Bögle, C., 2006. Gradual failure in fibre/polymer laminates. Compos. Sci. Technol. 66, 616–625.

Kriz, R.D., Stinchcomb, W.W., 1979. Exp. Mech. 19, 41.

Lee, H.K., Kim, B.R., 2007. Numerical characterization of compressive response and damage evolution in laminated plates containing a cutout. Compos. Sci. Technol. 67, 2221–2230.

Liang, Z., Lee, H.K., Suaris, W., 2006. Micromechanics-based constitutive modeling for unidirectional laminated composites. Int. J. Solids Struct. 43, 5674–5689.

Luccioni, B., Oller, S., Danesi, R., 1995. Plastic damaged model for anisotropic materials. Appl. Mech. Am. I, 124–129.

Luccioni, B., Oller, S., Danesi, R., 1996. Coupled plastic-damaged model. Comput. Meth. Appl. Mech. Eng. 129, 81–89.

Luccioni, B., Martín, P.E., 1997. Modelo elastoplástico para materiales ortótropos. Rev. Int. Mét. Num. Dis, Cálc. Ing. 13 (4), 603–614.

Luccioni, B., López, D., 2002. Modelo para Materiales Compuestos con deslizamiento de Fibras. In: Oller, S. (Ed), Análisis y Cálculo de Estructuras de Materiales Compuestos. CIMNE, Barcelona, España, pp. 411–431 (Chap. 13).

Luccioni, B., López, D., Danesi, R., 2005. Bond slip in reinforced concrete elements. J. Struct. Eng.-ASCE 131 (11), 571–574.

Luccioni, B., 2006. Constitutive model for fibre reinforced composite laminates. J. Appl. Mech.-T ASME 73 (6), 901–910.

Maimí, P., Camanho, P.P., Mayugo, J.A., Dávila, C.G., 2007a. A continuum damage model for composite laminates: Part I – Constitutive model. Mech. Mater. 39 (10), 897–908.

Maimí, P., Camanho, P.P., Mayugo, J.A., Dávila, C.G., 2007b. A continuum damage model for composite laminates: Part II – Computational implementation and validation. Mech. Mater. 39 (10), 909–919.

Mori, T., Tanaka, K., 1973. Average stress in matrix and average elastic energy of materials with misfitting inclusions. Acta Metall. 21, 571–574.

Narayana Naik, G., Krishna Murty, A.V., Gopalakrishnan, S., 2005. A failure mechanism based failure theory for laminated composites including the effect of shear stress. Compos. Struct. 69, 219–227.

Oller, S., Botello, S., Miquel, M., Oñate, E., 1995. Anisotropic elasto-plastic model based on an isotropic formulation. Eng. Comput. 12, 245–262.

Oller, S., Car, E., Lubliner, J., 2003. Definition of a general implicit orthotropic yield criterion. Comput. Meth. Appl. Mech. Eng. 192, 895–912.

Oller, S., Miquel, J., Zalamea, J., 2005. Composite material behavior using a homogenization double scale method. J. Eng. Mech., ASCE 131, 65–79.

Schuecker, C., Pettermann, H.E., 2006. A continuum damage model for fiber reinforced laminates based on ply failure mechanisms. Compos. Struct. 76, 162–173.

Sihn, S., Kim, R., Kawabe, K., Tsai, S., 2007. Experimental studies of thin-ply laminated composites. Compos. Sci. Technol. 67, 996–1008.

Soden, P.D., Hinton, M.J., Kaddour, A.S., 1998a. Lamina properties, lay-up configurations and loading conditions for a range of fiber-reinforced composite laminates. Compos. Sci. Technol. 58, 1011–1022.

Soden, P.D., Hinton, M.J., Kaddour, A.S., 1998b. A comparison of the predictive capabilities of current failure theories for composite laminates. Compos. Sci. Technol. 58, 1225–1254.

Soden, P.D., Hinton, M.J., Kaddour, A.S., 2002. Biaxial test results for strength and deformation of a range of E-glass and carbon fiber reinforced composite laminates: failure exercise benchmark data. Compos. Sci. Technol. 62, 1489–1514.

Soden, P.D., Kaddour, A.S., Hinton, M.J., 2004. Recommendations for designers and researchers resulting from the world-wide failure exercise. Compos. Sci. Technol. 64, 589–604.

Tandon, G.P., Weng, G.J., 1984. The effect of aspect ratio of inclusions on the elastic properties of unidirectionally aligned composites. Polym. Compos. 5, 327–333.

Tay-Earn, T., Tan, V., Liu, G., 2006. A new integrated micro–macro approach to damage and fracture of composites. Mat. Sci. Eng. B 132, 138–142.

Tsai, S.W., Hahn, H.T., 1980. Introduction to Composite Materials. Technomic Publishing, Lancaster.

Wang, A.S.D., Yan, K.C.K., 2005. On modeling matrix failures in composites. Composites: Part A 36, 1335–1346.

Yokozeki, T., Ogihara, S., Yoshida, S., Ogasawara, T., 2007. Simple constitutive model for nonlinear response of fiber-reinforced composites with loading-directional dependence. Compos. Sci. Technol. 67, 111–118.

Zhu, L., Chattopadhyay, A., Goldberg, R.K., 2006. Nonlinear transient response of strain rate dependent composite laminated plates using multiscale simulation. Int. J. Solids Struct. 43, 2602–2630.